Eur. Phys. J. C (2017) 77:190
DOI 10.1140/epjc/s10052-017-4748-2

THE EUROPEAN PHYSICAL JOURNAL C

Regular Article - Theoretical Physics

$B^0 \to K^{*0}\mu^+\mu^-$ decay in the aligned two-Higgs-doublet model

Quan-Yi Hu[a], **Xin-Qiang Li**[b], **Ya-Dong Yang**[c]

Institute of Particle Physics and Key Laboratory of Quark and Lepton Physics (MOE), Central China Normal University, Wuhan 430079, Hubei, China

Received: 3 January 2017 / Accepted: 9 March 2017 / Published online: 25 March 2017

Abstract In the aligned two-Higgs-doublet model, we perform a complete one-loop computation of the short-distance Wilson coefficients $C^{(\prime)}_{7,9,10}$, which are the most relevant ones for $b \to s\ell^+\ell^-$ transitions. It is found that, when the model parameter $|\varsigma_u|$ is much smaller than $|\varsigma_d|$, the charged scalar contributes mainly to chirality-flipped $C'_{9,10}$, with the corresponding effects being proportional to $|\varsigma_d|^2$. Numerically, the charged-scalar effects fit into two categories: (A) $C^{\mathrm{H}^\pm}_{7,9,10}$ are sizable, but $C'^{\mathrm{H}^\pm}_{9,10} \simeq 0$, corresponding to the (large $|\varsigma_u|$, small $|\varsigma_d|$) region; (B) $C^{\mathrm{H}^\pm}_7$ and $C'^{\mathrm{H}^\pm}_{9,10}$ are sizable, but $C^{\mathrm{H}^\pm}_{9,10} \simeq 0$, corresponding to the (small $|\varsigma_u|$, large $|\varsigma_d|$) region. Taking into account phenomenological constraints from the inclusive radiative decay $B \to X_s\gamma$, as well as the latest model-independent global analysis of $b \to s\ell^+\ell^-$ data, we obtain the much restricted parameter space of the model. We then study the impact of the allowed model parameters on the angular observables P_2 and P'_5 of $B^0 \to K^{*0}\mu^+\mu^-$ decay, and we find that P'_5 could be increased significantly to be consistent with the experimental data in case B.

1 Introduction

The rare $B \to K^*\ell^+\ell^-$ decays, being the flavor-changing neutral-current (FCNC) processes, do not arise at tree level and are highly suppressed at higher orders within the Standard Model (SM), due to the Glashow–Iliopoulos–Maiani (GIM) mechanism [1]. However, new TeV-scale particles in many extensions of the SM could affect the decay amplitude at a similar level as the SM does. These decays play, therefore, a crucial role in testing the SM and probing various NP scenarios beyond it [2]. It is particularly interesting to note that, based on these decays, observables with a very limited sensitivity to hadronic uncertainties can be constructed, enhancing therefore the discovery potential for NP [3–10].

Experimentally, several interesting deviations from the SM predictions have been observed in these decays. In 2013, the form-factor-independent angular observable P'_5 [8,9] of $B^0 \to K^{*0}\mu^+\mu^-$ decay was measured by the LHCb collaboration [11], showing a 3.7σ disagreement with the SM expectation [12–15]. Recently, the LHCb collaboration has released new measurements of the angular observables in this decay, based on the dataset of 3 fb^{-1} of integrated luminosity, and still found a 3.4σ deviation for P'_5 [16]. Moreover, being in agreement with the LHCb measurements, a deviation with a significance of 2.1σ was also reported by the Belle collaboration [17]. Besides the P'_5 anomaly, there are some other slight deviations beyond the 2σ level, such as the observables P_2 in $q^2 \in [2, 4.3]$ GeV^2 and P'_4 in $q^2 \in [14.18, 16]$ GeV^2 [18–20]. These anomalies have triggered lots of theoretical studies both within the SM and in various NP models [8–10,12–15,18–44].

As a minimal extension of the SM scalar sector, the two-Higgs-doublet model (2HDM) [45] can easily satisfy the electroweak (EW) precision data and, at the same time, lead to a very rich phenomenology [46]. The scalar spectrum consists of two charged scalars $H^\pm$ and three neutral ones h, H, and A, one of which is to be identified with the SM-like Higgs boson found at the LHC [47,48]. The direct search for these additional scalar states would be an important task for high-energy colliders in the next few years. It should be noted that, complementary to the direct searches, indirect constraints on the 2HDM could also be obtained from the rare FCNC decays like $B \to K^*\ell^+\ell^-$, since these scalars can affect these processes through the penguin and box diagrams. These studies are also very helpful to gain further insights into the scalar sector of supersymmetry and other models that have similar scalar contents [49–51].

In a generic 2HDM, the non-diagonal couplings of neutral scalars to fermions lead to tree-level FCNC interactions, which can be avoided by imposing on the Lagrangian an

[a] e-mail: qyhu@mails.ccnu.edu.cn
[b] e-mail: xqli@mail.ccnu.edu.cn
[c] e-mail: yangyd@mail.ccnu.edu.cn

ad hoc discrete $\mathcal{Z}_2$ symmetry. Depending on the $\mathcal{Z}_2$ charge assignments to the scalars and fermions, this results in four types of 2HDMs (types I, II, X, Y) [46,52] under the hypothesis of natural flavor conservation (NFC) [53]. In the aligned two-Higgs-doublet model (A2HDM) [54], on the other hand, the absence of tree-level FCNCs is automatically guaranteed by assuming the alignment in flavor space of the Yukawa matrices for each type of right-handed fermions. Interestingly, the A2HDM can recover as particular cases all known specific implementations of the 2HDMs based on $\mathcal{Z}_2$ symmetries. The model also features possible new sources of CP violation beyond that of the Cabibbo–Kobayashi–Maskawa (CKM) matrix [55,56]. These features make the A2HDM very attracting both in high-energy collider physics [57–63] and in low-energy flavor physics [64–74].

In this paper, we will study the decay $B^0 \to K^{*0}\mu^+\mu^-$ in the A2HDM. Our paper is organized as follows: in Sect. 2, we give a brief overview of the A2HDM, focusing mainly on the scalar and Yukawa sectors. In Sect. 3, a complete one-loop computation of the short-distance (SD) Wilson coefficients $C_{7,9,10}^{(\prime)}$ is presented, and the final analytical expressions are given both within the SM and in the A2HDM. The angular observables of $B^0 \to K^{*0}\mu^+\mu^-$ decay are also introduced in this section. In Sect. 4, taking into account phenomenological constraints from the inclusive radiative decay $B \to X_s\gamma$ and the latest model-independent global analysis of $b \to s\ell^+\ell^-$ data, we study the impact of the allowed model parameters on the angular observables P_2 and P_5' of $B^0 \to K^{*0}\mu^+\mu^-$ decay. Finally, our conclusions are drawn in Sect. 5. Some relevant functions for the Wilson coefficients are collected in the appendices.

2 The aligned two-Higgs-doublet model

We consider the minimal version of 2HDM, which is invariant under the SM gauge group and includes, besides the SM matter and gauge fields, two complex scalar $SU(2)_L$ doublets,

$$\phi_a^{\mathrm{T}}(x) = \frac{e^{i\theta_a}}{\sqrt{2}}(\sqrt{2}\varphi_a^+,\ v_a + \rho_a + i\eta_a), \quad (a = 1,\ 2)\,, \tag{2.1}$$

with the hypercharge $Y = 1/2$. The neutral components of the two scalar doublets acquire the vacuum expectation values (VEVs) $\langle 0|\phi_a^{\mathrm{T}}(x)|0\rangle = (0, v_a e^{i\theta_a}/\sqrt{2})$. Through an appropriate $U(1)_Y$ transformation, one can enforce $\theta_1 = 0$ and leave the relative phase $\theta = \theta_2 - \theta_1$ as physical. Using further a global $SU(2)$ transformation in the scalar space, one can rotate the original scalar basis to the so-called Higgs basis [75–77],

$$\begin{pmatrix} \Phi_1 \\ -\Phi_2 \end{pmatrix} \equiv \begin{pmatrix} \cos\beta & \sin\beta \\ \sin\beta & -\cos\beta \end{pmatrix} \begin{pmatrix} \phi_1 \\ e^{-i\theta}\phi_2 \end{pmatrix}, \tag{2.2}$$

where the rotation angle (clockwise) $\tan\beta = v_2/v_1$. In the new basis, only the scalar doublet Φ_1 gets a nonzero VEV $\langle 0|\Phi_1^{\mathrm{T}}(x)|0\rangle = (0, v/\sqrt{2})$, with $v = \sqrt{v_1^2 + v_2^2} = (\sqrt{2}G_F)^{-1/2} \simeq 246$ GeV, and the two scalar doublets are now parametrized, respectively, by [54]

$$\Phi_1 = \begin{pmatrix} G^+ \\ \frac{1}{\sqrt{2}}(v + S_1 + iG^0) \end{pmatrix}, \quad \Phi_2 = \begin{pmatrix} H^+ \\ \frac{1}{\sqrt{2}}(S_2 + iS_3) \end{pmatrix}, \tag{2.3}$$

where $G^\pm$ and G^0 denote the massless Goldstone fields to be eaten by the $W^\pm$ and Z^0 gauge bosons, respectively. The remaining five physical degrees of freedom are given by the two charged fields $H^\pm(x)$ and the three neutral ones $\varphi_i^0(x) = \{h(x), H(x), A(x)\} = \mathcal{R}_{ij}S_j$, where $\mathcal{R}$ is an orthogonal matrix obtained after diagonalizing the mass terms in the scalar potential. Generally, none of these three neutral scalars can have a definite CP quantum number.

2.1 Scalar sector

The most general scalar potential for the two doublets Φ_1 and Φ_2 that is allowed by the EW gauge symmetry can be written as [75–77]

$$\begin{aligned} V = {} & \mu_1(\Phi_1^\dagger\Phi_1) + \mu_2(\Phi_2^\dagger\Phi_2) + [\mu_3(\Phi_1^\dagger\Phi_2) + \mu_3^*(\Phi_2^\dagger\Phi_1)] \\ & + \lambda_1(\Phi_1^\dagger\Phi_1)^2 + \lambda_2(\Phi_2^\dagger\Phi_2)^2 + \lambda_3(\Phi_1^\dagger\Phi_1)(\Phi_2^\dagger\Phi_2) \\ & + \lambda_4(\Phi_1^\dagger\Phi_2)(\Phi_2^\dagger\Phi_1) \\ & + [(\lambda_5\,\Phi_1^\dagger\Phi_2 + \lambda_6\,\Phi_1^\dagger\Phi_1 + \lambda_7\,\Phi_2^\dagger\Phi_2)(\Phi_1^\dagger\Phi_2) + \text{h.c.}]. \end{aligned} \tag{2.4}$$

The hermiticity of the potential requires the parameters $\mu_{1,2}$ and $\lambda_{1,2,3,4}$ to be real, while μ_3 and $\lambda_{5,6,7}$ could be generally complex. The minimization condition imposes the relations $\mu_1 = -\lambda_1 v^2$ and $\mu_3 = -\frac{1}{2}\lambda_6 v^2$. Since only the relative phases among $\lambda_{5,6,7}$ are physical, the scalar potential is finally fully characterized by 11 real parameters, v, μ_2, $\lambda_{1,2,3,4}$, $|\lambda_{5,6,7}|$, $\arg(\lambda_5\lambda_6^*)$ and $\arg(\lambda_5\lambda_7^*)$, four of which can be determined by the scalar masses $M_{H^\pm, h, H, A}$. Explicitly, inserting Eq. (2.3) into Eq. (2.4) and imposing the minimization condition, one gets $M_{H^\pm}^2 = \mu_2 + \frac{1}{2}\lambda_3 v^2$, and the mass-squared matrix $\mathcal{M}^2$ of $S_{1,2,3}$ fields in terms of v and λ_i. Using the orthogonal matrix $\mathcal{R}$, one can then obtain the masses of the three neutral scalars, $\mathcal{R}\,\mathcal{M}^2\,\mathcal{R}^{\mathrm{T}} = \mathrm{diag}\left(M_h^2, M_H^2, M_A^2\right)$.

In the CP-conserving limit, $\lambda_{5,6,7}$ are all real and the neutral scalars are CP eigenstates. The CP-odd scalar A corresponds to S_3, with the mass given by $M_A^2 = M_{H^\pm}^2 + v^2\left(\frac{\lambda_4}{2} - \lambda_5\right)$, while the two CP-even scalars h and H are orthogonal combinations of S_1 and S_2,

$$\begin{pmatrix} h \\ H \end{pmatrix} = \begin{pmatrix} \cos\tilde{\alpha} & \sin\tilde{\alpha} \\ -\sin\tilde{\alpha} & \cos\tilde{\alpha} \end{pmatrix} \begin{pmatrix} S_1 \\ S_2 \end{pmatrix}, \tag{2.5}$$

where the mixing angle $\tilde{\alpha}$ is determined by

$$\tan\tilde{\alpha} = \frac{M_h^2 - 2\lambda_1 v^2}{v^2\lambda_6} = \frac{v^2\lambda_6}{2\lambda_1 v^2 - M_H^2}. \tag{2.6}$$

The masses of the two neutral scalars are given, respectively, by $M_h^2 = \frac{1}{2}(\Sigma - \Delta)$ and $M_H^2 = \frac{1}{2}(\Sigma + \Delta)$, where

$$\begin{aligned} \Sigma &= M_{H^\pm}^2 + v^2\left(2\lambda_1 + \frac{\lambda_4}{2} + \lambda_5\right), \\ \Delta &= \sqrt{\left[M_{H^\pm}^2 + v^2\left(-2\lambda_1 + \frac{\lambda_4}{2} + \lambda_5\right)\right]^2 + 4v^4\lambda_6^2} \\ &= -\frac{2v^2\lambda_6}{\sin(2\tilde{\alpha})}. \end{aligned} \tag{2.7}$$

Here $M_h \leqslant M_H$ by convention and the SM limit is recovered when $\tilde{\alpha} = 0$.

2.2 Yukawa sector

The Yukawa Lagrangian of the 2HDM is most generally given by [46,54]

$$\begin{aligned} \mathcal{L}_Y = &-[\bar{Q}'_L(\Gamma_1\phi_1 + \Gamma_2\phi_2)d'_R + \bar{Q}'_L(\Delta_1\tilde{\phi}_1 + \Delta_2\tilde{\phi}_2)u'_R \\ &+\bar{L}'_L(\Pi_1\phi_1 + \Pi_2\phi_2)\ell'_R] + \text{h.c.}, \end{aligned} \tag{2.8}$$

where $\tilde{\phi}_a(x) \equiv i\tau_2\phi_a^*(x)$ are the charge-conjugated fields with $Y = -\frac{1}{2}$, $\bar{Q}'_L$ and $\bar{L}'_L$ are the left-handed quark and lepton doublets, and u'_R, d'_R and ℓ'_R the corresponding right-handed singlets, in the weak-interaction basis. All fermionic fields are written as 3-dimensional vectors and the couplings Γ_a, Δ_a and Π_a are therefore 3×3 complex matrices in flavor space.

Transforming to the Higgs basis, Eq. (2.8) becomes

$$\begin{aligned} \mathcal{L}_Y = &-\frac{\sqrt{2}}{v}[\bar{Q}'_L(M'_d\Phi_1 + Y'_d\Phi_2)d'_R + \bar{Q}'_L(M'_u\tilde{\Phi}_1 \\ &+Y'_u\tilde{\Phi}_2)u'_R + \bar{L}'_L(M'_\ell\Phi_1 + Y'_\ell\Phi_2)\ell'_R] + \text{h.c.}, \end{aligned} \tag{2.9}$$

where

$$M'_d = \frac{1}{\sqrt{2}}(v_1\Gamma_1 + v_2\Gamma_2 e^{i\theta}), \qquad Y'_d = \frac{1}{\sqrt{2}}(-v_2\Gamma_1 + v_1\Gamma_2 e^{i\theta}), \tag{2.10}$$

$$M'_u = \frac{1}{\sqrt{2}}(v_1\Delta_1 + v_2\Delta_2 e^{-i\theta}), \quad Y'_u = \frac{1}{\sqrt{2}}(-v_2\Delta_1 + v_1\Delta_2 e^{-i\theta}), \tag{2.11}$$

$$M'_\ell = \frac{1}{\sqrt{2}}(v_1\Pi_1 + v_2\Pi_2 e^{i\theta}), \qquad Y'_\ell = \frac{1}{\sqrt{2}}(-v_2\Pi_1 + v_1\Pi_2 e^{i\theta}). \tag{2.12}$$

Table 1 The one-to-one correspondence between different specific choices of the couplings ς_f and the 2HDMs based on discrete $\mathcal{Z}_2$ symmetries

Model	ς_d	ς_u	ς_ℓ
Type I	$\cot\beta$	$\cot\beta$	$\cot\beta$
Type II	$-\tan\beta$	$\cot\beta$	$-\tan\beta$
Type X	$\cot\beta$	$\cot\beta$	$-\tan\beta$
Type Y	$-\tan\beta$	$\cot\beta$	$\cot\beta$
Inert	0	0	0

In general, the Yukawa matrices M'_f and Y'_f ($f = u, d, \ell$) cannot be simultaneously diagonalized in flavor space. Thus, in the mass-eigenstate basis, with diagonal fermion mass matrices M_f, the corresponding Yukawa matrices Y_f remain non-diagonal, giving rise to tree-level FCNC interactions. The unwanted tree-level FCNCs can be eliminated by requiring the alignment in flavor space of the Yukawa matrices [54]:

$$\begin{aligned} &\Gamma_2 = \xi_d\, e^{-i\theta}\,\Gamma_1, \quad \Delta_2 = \xi_u^*\, e^{i\theta}\Delta_1, \quad \Pi_2 = \xi_\ell\, e^{-i\theta}\,\Pi_1, \\ &Y_{d,\ell} = \varsigma_{d,\ell}\, M_{d,\ell}, \quad Y_u = \varsigma_u^*\, M_u, \quad \varsigma_f \equiv \frac{\xi_f - \tan\beta}{1 + \xi_f\tan\beta}, \end{aligned} \tag{2.13}$$

where ξ_f (ς_f) are arbitrary complex parameters and could introduce new sources of CP violation beyond that of the CKM matrix.

The interactions of the charged scalar with the fermion mass-eigenstate fields then read

$$\begin{aligned} \mathcal{L}_{H^\pm} = &-\frac{\sqrt{2}}{v}H^+\{\bar{u}[\varsigma_d\, V_{\text{CKM}}M_d P_R - \varsigma_u\, M_u^\dagger V_{\text{CKM}} P_L]d \\ &+\varsigma_\ell\,\bar{\nu}M_\ell P_R\ell\} + \text{h.c.}, \end{aligned} \tag{2.14}$$

where $P_{L(R)} \equiv (1 \mp \gamma_5)/2$ is the left (right)-handed chirality projector, and V_{CKM} the CKM matrix [55,56]. Here we did not give the neutral scalar sector [54] in $\mathcal{L}_Y$ or the FCNC local structures induced beyond tree level (quantum corrections) [64], because their effects are highly suppressed by the muon mass in the decay $B^0 \to K^{*0}\mu^+\mu^-$. The usual NFC models [46,52], with discrete $\mathcal{Z}_2$ symmetries, are recovered for particular values of ς_f, as shown in Table 1.

3 $B^0 \to K^{*0}\mu^+\mu^-$ in the A2HDM

3.1 Effective weak Hamiltonian

The rare decay $B^0 \to K^{*0}\mu^+\mu^-$ proceeds through the loop diagrams both within the SM and in the A2HDM. When the heavy degrees of freedom, including the top quark, the weak gauge bosons, as well as the charged scalars, have been integrated out, we obtain the low-energy effective weak Hamiltonian governing the decay [6,78]:

$$\mathcal{H}_{\rm eff} = -\frac{4G_F}{\sqrt{2}} V_{tb}V_{ts}^* \sum_i (C_i O_i + C_i' O_i'), \tag{3.1}$$

where G_F is the Fermi coupling constant. Here we neglect the doubly Cabibbo-suppressed contributions to Eq. (3.1) (proportional to $V_{ub}V_{us}^*$), and we focus only on the operators [6]

$$O_7 = \frac{e}{16\pi^2}\bar{m}_b(\bar{s}\sigma^{\mu\nu}P_R b)F_{\mu\nu}, \quad O_7' = \frac{e}{16\pi^2}\bar{m}_b(\bar{s}\sigma^{\mu\nu}P_L b)F_{\mu\nu}, \tag{3.2}$$

$$O_9 = \frac{e^2}{16\pi^2}(\bar{s}\gamma^\mu P_L b)(\bar{\mu}\gamma_\mu \mu), \quad O_9' = \frac{e^2}{16\pi^2}(\bar{s}\gamma^\mu P_R b)(\bar{\mu}\gamma_\mu \mu), \tag{3.3}$$

$$O_{10} = \frac{e^2}{16\pi^2}(\bar{s}\gamma^\mu P_L b)(\bar{\mu}\gamma_\mu\gamma_5 \mu), \quad O_{10}' = \frac{e^2}{16\pi^2}(\bar{s}\gamma^\mu P_R b)(\bar{\mu}\gamma_\mu\gamma_5 \mu), \tag{3.4}$$

where $\bar{m}_b = \bar{m}_b(\mu)$ denotes the b-quark running mass in the $\overline{\rm MS}$ scheme.

Within the SM, the electromagnetic dipole operator O_7 and the semileptonic operators $O_{9,10}$ play the leading role in the decay $B^0 \to K^{*0}\mu^+\mu^-$. Besides modifying the values of the SD Wilson coefficients $C_{7,9,10}$, the charged-scalar contributions could also make the chirality-flipped operators $O'_{7,9,10}$ defined above to contribute in a significant manner, especially in some regions of the parameter spaces discussed later.

The SD Wilson coefficients $C_i(\mu)$ and $C_i'(\mu)$ can be obtained firstly at the matching scale $\mu_W \sim M_W$ perturbatively, by requiring equality of the one-particle irreducible Green functions calculated in the full and in the effective theory [78]. Using the renormalization group equation, one can then get $C_i(\mu)$ and $C_i'(\mu)$ at the lower scale $\mu_b \sim m_b$. During the calculation, the limit $\bar{m}_{u,c} \to 0$ and the unitarity of the CKM matrix have been used. For simplicity, we introduce the mass ratios:

$$x_t = \frac{\bar{m}_t^2(\mu_W)}{M_W^2}, \quad y_t = \frac{\bar{m}_t^2(\mu_W)}{M_{H^\pm}^2}. \tag{3.5}$$

Details of the computational method could be found, for example, in Refs. [70,78].

3.2 Wilson coefficients in the SM

In the SM, the one-loop penguin and box diagrams have been calculated both in the Feynman ($\xi = 1$) and in the unitary ($\xi = \infty$) gauge [79–87], denoted by the subscript 'F' and 'U', respectively. The different contributions to $C_i^{\rm SM}(\mu_W)$ can be split into the following forms:

$$C_7^{\rm SM} = C_7^{\gamma\text{-penguin}}, \tag{3.6}$$

$$C_9^{\rm SM} = C_9^{W\text{-box}} + C_9^{Z\text{-penguin}} + C_9^{\gamma\text{-penguin}}, \tag{3.7}$$

$$C_{10}^{\rm SM} = C_{10}^{W\text{-box}} + C_{10}^{Z\text{-penguin}}, \tag{3.8}$$

where the corresponding parts resulting from the W-box, Z-penguin and γ-penguin diagrams are given, respectively, by

$$C_{9,\rm F(U)}^{W\text{-box}} = -\frac{B_{0,\rm F(U)}}{\sin^2\theta_W}, \quad C_{10,\rm F(U)}^{W\text{-box}} = \frac{B_{0,\rm F(U)}}{\sin^2\theta_W}, \tag{3.9}$$

$$C_{9,\rm F(U)}^{Z\text{-penguin}} = \left(-4 + \frac{1}{\sin^2\theta_W}\right) C_{0,\rm F(U)}, \quad C_{10,\rm F(U)}^{Z\text{-penguin}} = -\frac{C_{0,\rm F(U)}}{\sin^2\theta_W}, \tag{3.10}$$

$$C_{7,\rm F(U)}^{\gamma\text{-penguin}} = -\frac{1}{2}D'_{0,\rm F(U)}, \quad C_{9,\rm F(U)}^{\gamma\text{-penguin}} = -D_{0,\rm F(U)} + \frac{4}{9}, \tag{3.11}$$

where θ_W is the Weinberg mixing angle, and the Inami–Lim functions [79] are defined as

$$\begin{aligned} B_{0,\rm F} &= F_1(x_t), \quad C_{0,\rm F} = F_3(x_t), \quad D'_{0,\rm F} = F_6(x_t), \\ D_{0,\rm F} &= -\frac{4}{9}F_0(x_t) + F_5(x_t), \end{aligned} \tag{3.12}$$

in the Feynman gauge, and

$$\begin{aligned} B_{0,\rm U} &= -\frac{x_t}{16}L_\epsilon + F_4(x_t), \\ C_{0,U} &= -\frac{x_t}{16}L_\epsilon - F_1(x_t) + F_3(x_t) + F_4(x_t), \\ D'_{0,\rm U} &= F_6(x_t), \\ D_{0,\rm U} &= \frac{x_t}{4}L_\epsilon - \frac{4}{9}F_0(x_t) + 4F_1(x_t) - 4F_4(x_t) + F_5(x_t), \end{aligned} \tag{3.13}$$

in the unitary gauge. Here we introduce the notation $L_\epsilon \equiv \frac{1}{\epsilon} + \log\left(\frac{\mu_W^2}{M_W^2}\right)$, where $\epsilon = (4-d)/2$ is the dimensional regulator of ultraviolet divergence. Explicit expressions of the basic functions $F_i(x)$ are given by Eqs. (A.1)–(A.9). While each piece on the right-hand side of Eqs. (3.7) and (3.8) depends obviously on ϵ in the unitary gauge, due to the longitudinal components of the $W^\pm$, Z^0 and off-shell photon propagators, the physical quantities $C_{7,9,10}^{\rm SM}$ are indeed free of ϵ and are independent of the EW gauge fixings. For a recent review of higher-order corrections to $C_{7,9,10}^{\rm SM}$, the reader is referred to Ref. [88].

3.3 Wilson coefficients in the A2HDM

In the A2HDM, the charged-scalar exchanges lead to additional contributions to $C_{7,9,10}$ and could also make the chirality-flipped operators $O'_{7,9,10}$ to contribute in a significant manner, through the Z^0- and γ-penguin diagrams shown in Fig. 1. Since we have neglected the light lepton mass, there is no contribution from the SM W-box diagrams with the $W^\pm$ bosons replaced by the charged scalars $H^\pm$.

For each Feynman diagram shown in Fig. 1, the contributions are identical in the two gauges. The total Wilson coefficients $C_{7,9,10}$ are split into two parts, one is from the SM contributions $C_{7,9,10}^{\rm SM}$, and the other from the charged-scalar ones

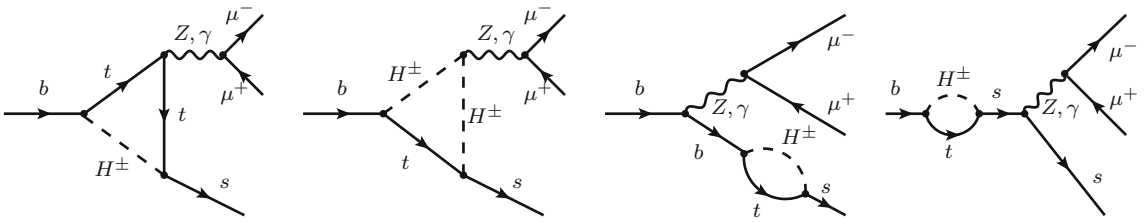

Fig. 1 Z- and γ-penguin diagrams involving the charged-scalar exchanges in the A2HDM

$C_{7,9,10}^{\mathrm{H}^\pm}$. For the chirality-flipped operators, $C'_{7,9,10} = C'^{\mathrm{H}^\pm}_{7,9,10}$, because the SM contributions are well suppressed by the factor $\bar{m}_s/\bar{m}_b$. For convenience, we decompose these new contributions in such a way as to render explicit their dependence on the couplings ς_u and ς_d:

$$C_7^{\mathrm{H}^\pm} = |\varsigma_u|^2\, C_{7,\,\mathrm{uu}} + \varsigma_d \varsigma_u^* C_{7,\,\mathrm{ud}}, \tag{3.14}$$

$$C_9^{\mathrm{H}^\pm} = |\varsigma_u|^2\, C_{9,\,\mathrm{uu}}, \tag{3.15}$$

$$C_{10}^{\mathrm{H}^\pm} = |\varsigma_u|^2\, C_{10,\,\mathrm{uu}}, \tag{3.16}$$

$$C_7'^{\mathrm{H}^\pm} = \frac{\bar{m}_s}{\bar{m}_b}\left(|\varsigma_u|^2\, C_{7,\,\mathrm{uu}} + \varsigma_u \varsigma_d^* C_{7,\,\mathrm{ud}}\right), \tag{3.17}$$

$$\begin{aligned} C_9'^{\mathrm{H}^\pm} &= \left(-1 + 4\sin^2\theta_W\right) C_{10}'^{\mathrm{H}^\pm} \\ &\quad + \frac{\bar{m}_b \bar{m}_s}{M_W^2}[|\varsigma_u|^2\, C'_{9,\,\mathrm{uu}} + 2\Re\left(\varsigma_u \varsigma_d^*\right) C'_{9,\,\mathrm{ud}} \\ &\quad + |\varsigma_d|^2\, C'_{9,\,\mathrm{dd}}], \end{aligned} \tag{3.18}$$

$$\begin{aligned} C_{10}'^{\mathrm{H}^\pm} &= \frac{\bar{m}_b \bar{m}_s}{M_W^2}[|\varsigma_u|^2\, C'_{10,\,\mathrm{uu}} + 2\Re\left(\varsigma_u \varsigma_d^*\right) C'_{10,\,\mathrm{ud}} \\ &\quad + |\varsigma_d|^2\, C'_{10,\,\mathrm{dd}}], \end{aligned} \tag{3.19}$$

where the coefficients of the different combinations of the couplings ς_u and ς_d are given by Eqs. (B.1)–(B.10). In the particular cases of type II and type Y 2HDMs with large $\tan\beta$, the only terms enhanced by a factor $\tan^2\beta$ originate from the $|\varsigma_d|^2$ part contributing only to $C'^{\mathrm{H}^\pm}_{9,10}$. The Wilson coefficients $C^{(\prime)\mathrm{H}^\pm}_{7,9,10}$ are found to be invariant under a global U(1) transformation, $\varsigma_u \to \mathrm{e}^{i\chi}\varsigma_u$ and $\varsigma_d \to \mathrm{e}^{i\chi}\varsigma_d$. This invariance is well anticipated, since it corresponds to an unphysical phase transformation of the second Higgs doublet, $\Phi_2 \to \mathrm{e}^{i\chi}\Phi_2$, a leftover freedom in the Higgs basis [75,76]. There is an implicit μ_W dependence via the s, b, t-quark masses, which depend on the precise definitions and have to be specified when going beyond the leading logarithm (LL). As we evaluate $C^{(\prime)\mathrm{H}^\pm}_{7,9,10}$ only at the leading order (LO) in α_s, whether the running masses $\bar{m}_q(\mu_W)$ or the pole masses m_q are used does not matter too much. As a consequence, we choose the pole masses m_q as input in Eqs. (3.17)–(3.19).

Our results for the chirality-flipped Wilson coefficients $C'^{\mathrm{H}^\pm}_{7,9,10}$ are presented for the first time in the A2HDM. In the particular cases of the $\mathcal{Z}_2$ symmetric 2HDMs, our results agree with the ones calculated in Refs. [89–92]. It is also noted that the next-to-leading order QCD corrections to $C^{\mathrm{H}^\pm}_{7,9,10}$ in the supersymmetry and type-II 2HDM have already been calculated in Refs. [93–97].

3.4 Angular observables in $B^0 \to K^{*0}\mu^+\mu^-$ decay

The angular distribution of the $B^0 \to K^{*0}(\to K^+\pi^-)\mu^+\mu^-$ decay is described by the dimuon invariant mass squared q^2 as well as the three angles θ_ℓ, θ_{K^*} and ϕ, where θ_ℓ is defined as the angle between the flight direction of the μ^+ (μ^-) and the opposite direction of the B^0 ($\bar{B}^0$) in the rest frame of the dimuon system, and θ_{K^*} the angle between the flight direction of the K^+ (K^-) and that of the B^0 ($\bar{B}^0$) in the K^{*0} ($\bar{K}^{*0}$) rest frame, while ϕ is the angle between the plane containing the dimuon pair and the plane containing K^+ and π^- mesons in the B^0 ($\bar{B}^0$) rest frame. In terms of these four kinematic variables, the full angular decay distribution of the decay is then given by [6,98]

$$\begin{aligned} &\frac{\mathrm{d}^4\bar{\Gamma}[B^0 \to K^{*0}\mu^+\mu^-]}{\mathrm{d}q^2\,\mathrm{d}\cos\theta_\ell\,\mathrm{d}\cos\theta_{K^*}\,\mathrm{d}\phi} \\ &= \frac{9}{32\pi}[\bar{I}_1^s \sin^2\theta_{K^*} + \bar{I}_1^c \cos^2\theta_{K^*} \\ &\quad + (\bar{I}_2^s \sin^2\theta_{K^*} + \bar{I}_2^c \cos^2\theta_{K^*})\cos 2\theta_\ell \\ &\quad + \bar{I}_3 \sin^2\theta_{K^*}\sin^2\theta_\ell \cos 2\phi + \bar{I}_4 \sin 2\theta_{K^*}\sin 2\theta_\ell \cos\phi \\ &\quad + \bar{I}_5 \sin 2\theta_{K^*}\sin\theta_\ell \cos\phi \\ &\quad + \bar{I}_6^s \sin^2\theta_{K^*}\cos\theta_\ell + \bar{I}_7 \sin 2\theta_{K^*}\sin\theta_\ell \sin\phi \\ &\quad + \bar{I}_8 \sin 2\theta_{K^*}\sin 2\theta_\ell \sin\phi + \bar{I}_9 \sin^2\theta_{K^*}\sin^2\theta_\ell \sin 2\phi], \end{aligned} \tag{3.20}$$

where the angular coefficients $\bar{I}_i^{(a)}$ are functions of q^2 only, and the relations $\bar{I}_1^s = 3\bar{I}_2^s$, $\bar{I}_1^c = -\bar{I}_2^c$ and $\bar{I}_6^c = 0$ hold when the muon mass is neglected. The corresponding expression for the CP-conjugated mode $\bar{B}^0 \to \bar{K}^{*0}(\to K^-\pi^+)\mu^+\mu^-$ is obtained from Eq. (3.20) by the replacements $\bar{I}_i^{(a)} \to I_i^{(a)}$ [6,98]. Explicit forms of the angular coefficients $\bar{I}_i^{(a)}$ ($I_i^{(a)}$) can be found, for example, in Refs. [6,10,16].

The self-tagging property of the decay $B^0 \to K^{*0}\mu^+\mu^-$ makes it possible to determine both the CP-averaged and the CP-asymmetric quantities defined, respectively, by [6]

$$S_i^{(a)} = (I_i^{(a)} + \bar{I}_i^{(a)}) \Big/ \left(\frac{\mathrm{d}\Gamma}{\mathrm{d}q^2} + \frac{\mathrm{d}\bar{\Gamma}}{\mathrm{d}q^2}\right),$$
$$A_i^{(a)} = (I_i^{(a)} - \bar{I}_i^{(a)}) \Big/ \left(\frac{\mathrm{d}\Gamma}{\mathrm{d}q^2} + \frac{\mathrm{d}\bar{\Gamma}}{\mathrm{d}q^2}\right). \tag{3.21}$$

The previously studied observables, such as the q^2 distributions of the forward–backward asymmetry $A_{\rm FB}$ and the CP asymmetry $A_{\rm CP}$, can be expressed in terms of these angular observables.

With the structure of the amplitudes at large recoil, it is possible to build clean observables whose sensitivity to the $B \to K^*$ transition form factors is suppressed by α_s or $\Lambda_{\rm QCD}/m_b$ [9]. These include the so-called P_i' and P_i observables defined by [9,99,100]

$$P_1 = \frac{S_3}{2S_2^s}, \quad P_2 = \frac{S_6^s}{8S_2^s}, \quad P_3 = \frac{S_9}{4S_2^s}, \tag{3.22}$$
$$P_4' = \frac{S_4}{2\sqrt{-S_2^s S_2^c}}, \quad P_5' = \frac{S_5}{2\sqrt{-S_2^s S_2^c}},$$
$$P_6' = \frac{S_7}{2\sqrt{-S_2^s S_2^c}}, \quad P_8' = \frac{S_8}{2\sqrt{-S_2^s S_2^c}}. \tag{3.23}$$

The numerical impact of charged-scalar contributions on some of these observables will be discussed in the next section.

4 Numerical results and discussions

4.1 Choice of the model parameters

For the considered decay $B^0 \to K^{*0}\mu^+\mu^-$, only three model parameters, the charged-scalar mass $M_{H^\pm}$ and the two alignment parameters ς_u and ς_d, are involved. In the following we assume the parameters $\varsigma_{u,d}$ to be real, indicating that the only source of CP violation in the A2HDM is still due to the CKM matrix. Following the previous studies, we now give the preset ranges of these model parameters:

- The charged-scalar mass is assumed to lie in the range $M_{H^\pm} \in [80, 1000]$ GeV, where the lower bound comes from the LEP direct search [101], while the upper bound from the unitarity and stability of the scalar potential [102–105].
- The alignment parameter ς_u is assumed to lie in the range $|\varsigma_u| \le 2$, to be compatible with the current data of loop-induced processes, such as $Z \to b\bar{b}$, $b \to s\gamma$, $B^0_{s,d}$–$\bar{B}^0_{s,d}$ mixings, as well as the $h(125)$ decays [62,63,65–69].
- The alignment parameter ς_d is only mildly constrained through phenomenological requirements that involve additionally other model parameters. So we let it to be a free parameter.
- In the 2HDMs with discrete $\mathcal{Z}_2$ symmetries, the parameters ς_u and ς_d are not independent but are related to each other through the ratio of the VEVs $\tan\beta = v_2/v_1$. The upper limit for $\tan\beta$ also comes from the unitarity and stability of the scalar potential [102–105]; we assume here $\tan\beta \le 50$.

4.2 Constraints on the model parameters

For the other input parameters, we take $M_Z = 91.1876$ GeV, $M_W = 80.385$ GeV, $m_t = (174.2 \pm 1.4)$ GeV, $m_b = (4.78 \pm 0.06)$ GeV, and $\bar{m}_s(2\ \text{GeV}) = (96^{+8}_{-4})$ MeV [106]. Since $C_7'^{\rm H^\pm} = \bar{m}_s/\bar{m}_b C_7^{\rm H^\pm}$ and $\bar{m}_s \ll \bar{m}_b$, the contribution from O_7' will be safely neglected.

The Wilson coefficient $C_7^{\rm H^\pm}$ is severely constrained by the inclusive decay $B \to X_s\gamma$. The branching ratio of $B \to X_s\gamma$ measured by CLEO [107], Belle [108–110] and BaBar [111–113], lead to the combined average [114]

$$\mathcal{B}^{\rm exp}(B \to X_s\gamma)\big|_{E_\gamma > 1.6\ \text{GeV}} = (3.43 \pm 0.21_{\rm stat.} \pm 0.07_{\rm syst.}) \times 10^{-4}, \tag{4.1}$$

which is in good agreement with the updated SM prediction [115]

$$\mathcal{B}^{\rm SM}(B \to X_s\gamma)\big|_{E_\gamma > 1.6\ \text{GeV}} = (3.36 \pm 0.23) \times 10^{-4}. \tag{4.2}$$

It should be noted that the chromomagnetic dipole operator $O_8 = \frac{g_s}{16\pi^2}\bar{m}_b\,(\bar{s}\sigma^{\mu\nu}P_R T^a b)\,G^a_{\mu\nu}$ also plays an important role in the decay $B \to X_s\gamma$. However, at the LO in α_s, this operator contributes to $B \to X_s\gamma$ only via its mixing with O_7. It is then found that, at the matching scale $\mu_W = 160$ GeV, the Wilson coefficients $C_7^{\rm H^\pm}$ and $C_8^{\rm H^\pm}$ should fulfill the constraint [115]:

$$-0.0634 \le C_7^{\rm H^\pm}(\mu_W) + 0.242\, C_8^{\rm H^\pm}(\mu_W) \le 0.0464, \tag{4.3}$$

where $C_8^{\rm H^\pm} = |\varsigma_u|^2 C_{8,\,\rm uu} + \varsigma_d \varsigma_u^* C_{8,\,\rm ud}$ [89], with the functions $C_{8,\,\rm uu}$ and $C_{8,\,\rm ud}$ given, respectively, by Eqs. (B.11) and (B.12).

Under the constraint from Eq. (4.3), we show in Fig. 2 the allowed regions in the ς_u–ς_d plane ($\varsigma_d > 0$), with three representative values of the charged-scalar mass, $M_{H^\pm} = 80$, 300 and 500 GeV as benchmarks. The case with $\varsigma_d < 0$ is obtained from Fig. 2 with the changes $\varsigma_u \to -\varsigma_u$ and $\varsigma_d \to -\varsigma_d$. It is observed that the allowed range of ς_d becomes quite large when ς_u tends to 0; particularly, when $\varsigma_u = 0$, no constraint on ς_d is obtained, because in this

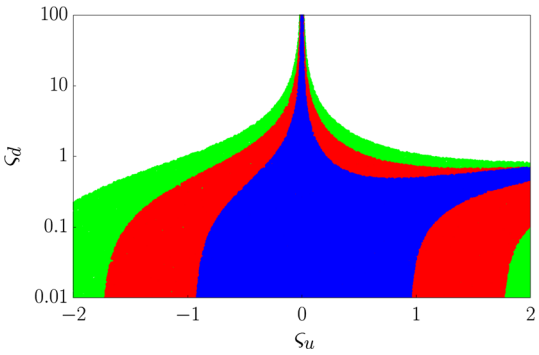

Fig. 2 The allowed regions in the ς_u–ς_d plane ($\varsigma_d > 0$) under the constraint from Eq. (4.3). The *blue*, *red*, and *green bands* correspond to $M_{H^\pm} = 80$, 300 and 500 GeV, respectively

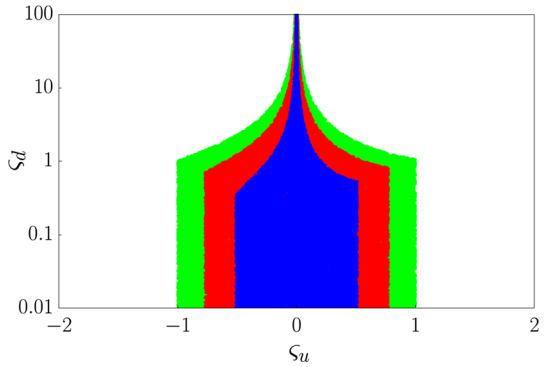

Fig. 3 The allowed regions in the ς_u–ς_d plane ($\varsigma_d > 0$) under the constraint from Eq. (4.3) as well as the bounds on $C_{9,10}^{\mathrm{H}^\pm}$ and $C_{9,10}^{\prime\mathrm{H}^\pm}$ from Eqs. (4.4) and (4.5). The other captions are the same as in Fig. 2

limit the SM result is recovered. When $\varsigma_d = 0$, on the other hand, a bound on ς_u can be set with the allowed range of $|\varsigma_u|$ further strengthened for smaller values of the charged-scalar mass. These qualitative observations are consistent with those observed previously in Refs. [64–66]. However, the allowed regions for ς_u and ς_d are further reduced compared to those obtained in Refs. [64–66], because the updated SM prediction (cf. Eq. (4.2)) becomes now more compatible with the current experimental data (cf. Eq. (4.1)). It is also found that the preset maximum value $|\varsigma_u| = 2$ is reached when $|\varsigma_d|$ varies within a range away from 0, rather than at $\varsigma_d = 0$; for example, taking $M_{H^\pm} = 80$ GeV, we find that $|\varsigma_u|$ approaches 2 when $0.6 < |\varsigma_d| < 0.8$. This novel observation motivates us to display the ς_d-axis in the logarithmic coordinate, making clear the correlation between ς_u and ς_d in the range $|\varsigma_d| < 1$. The inversely proportional and parabolic boundary curves in the first quadrant indicate that the NP contribution to $C_7^{\mathrm{H}^\pm}$ (cf. Eq. (3.14)) is dominated by the $\varsigma_d\varsigma_u^*$ and $|\varsigma_u|^2$ terms, respectively. As the large same-sign solutions for ς_u and ς_d obtained in Refs. [64,65], corresponding to the case when the NP influence is about twice the size of the SM contribution but with an opposite sign, are already excluded by the isospin asymmetry of $B \to K^*\gamma$ decays [66,116], they are not shown in Fig. 2.

Motivated by the latest LHCb and Belle measurements of $b \to s\ell^+\ell^-$ decays, there exist several global fits for the NP contributions to the Wilson coefficients $C_{9,10}^{(\prime)}$ [18–20,29]. We use two of these global fit results to further constrain the A2HDM parameters. One is obtained from the combined fit to the $b \to s\,(\mu^+\mu^-, \gamma)$ mesonic decays (at $\mu_b = 4.8$ GeV) [19]:

$$\begin{aligned} -2.2 \le C_9^{\mathrm{NP}} \le -0.4, \qquad & -0.5 \le C_{10}^{\mathrm{NP}} \le 2.0, \\ -1.3 \le C_9^{\prime\mathrm{NP}} \le 3.7, \qquad & -1.0 \le C_{10}^{\prime\mathrm{NP}} \le 1.6, \end{aligned} \tag{4.4}$$

given at the 3σ level. This fit includes the branching ratios and optimized angular observables of $B \to K^*\mu^+\mu^-$ and $B_s \to \phi\mu^+\mu^-$, the branching ratios of $B \to K\mu^+\mu^-$, the branching ratios of $B \to X_s\mu^+\mu^-$ (restricted only to the range $1\,\mathrm{GeV}^2 \le q^2 \le 6\,\mathrm{GeV}^2$) and $B \to X_s\gamma$, the branching ratio of $B_s \to \mu^+\mu^-$, as well as the isospin asymmetry and the time-dependent CP asymmetry of $B \to K^*\gamma$. Furthermore, both the large- and the low-recoil data are included for the exclusive $b \to s\mu^+\mu^-$ decays, resulting in nearly a hundred observables in total in the analysis [19]. The other global fit includes, besides the time-integrated branching ratio of $B_s \to \mu^+\mu^-$ and the branching ratio of $B \to X_s\ell^+\ell^-$ integrated over the range $1\,\mathrm{GeV}^2 \le q^2 \le 6\,\mathrm{GeV}^2$, the currently available data on $\Lambda_b \to \Lambda(\to p\pi^-)\,\mu^+\mu^-$ decay, which involves the branching ratio, the rate of longitudinally polarized lepton pair, as well as the leptonic and the hadronic forward–backward asymmetries; numerically, this fit gives (at $\mu_b = 4.2$ GeV) [29]

$$\begin{aligned} 0.9 \le C_9^{\mathrm{NP}} \le 2.5, \qquad & 1.8 \le C_{10}^{\mathrm{NP}} \le 4.2, \\ -1.3 \le C_9^{\prime\mathrm{NP}} \le 1.8, \qquad & 1.0 \le C_{10}^{\prime\mathrm{NP}} \le 3.1, \end{aligned} \tag{4.5}$$

at the 1σ level. It is interesting to note that the latter prefers a shift to C_9 that is opposite in sign compared to the former [29]. Since the Wilson coefficients $C_{9,10}^{\mathrm{H}^\pm}(\mu_W)$ and $C_{9,10}^{\prime\mathrm{H}^\pm}(\mu_W)$ are calculated only at the LO, they should be evolved to the lower scale μ_b at the LL approximation, which means that they are actually not running [117]. Thus, we can apply directly the bounds given by Eqs. (4.4) and (4.5) to $C_{9,10}^{\mathrm{H}^\pm}$ and $C_{9,10}^{\prime\mathrm{H}^\pm}$. To be more conservative, we require each of these coefficients to lie within the smaller lower and bigger upper bounds of these two global fits. Using these bounds as well as the constraint from Eq. (4.3), we find that the allowed parameter space in the ς_u–ς_d plane are significantly reduced, especially for the model parameter ς_u, as shown in Fig. 3. This means that $C_{9,10}^{\mathrm{H}^\pm}$ play a major role in the small $|\varsigma_d|$ region ($|\varsigma_d| < 1$) and $C_{9,10}^{\prime\mathrm{H}^\pm}$ can be quite sizable when ς_u approaches 0.

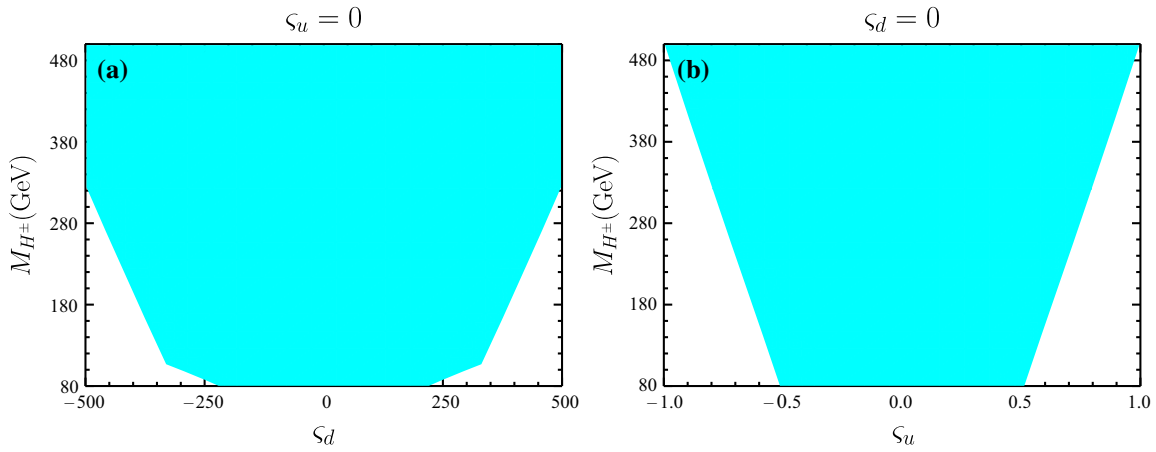

Fig. 4 The allowed regions in the ς_d–$M_{H^\pm}$ plane when $\varsigma_u = 0$ (**a**) and in the ς_u–$M_{H^\pm}$ plane when $\varsigma_d = 0$ (**b**), under the constraint from Eq. (4.3) as well as the bounds on $C_{9,10}^{\mathrm{H}^\pm}$ and $C_{9,10}^{\prime\mathrm{H}^\pm}$ from Eqs. (4.4) and (4.5)

It is also interesting to note that, under the constraint from Eq. (4.3) as well as the bounds on $C_{9,10}^{\mathrm{H}^\pm}$ and $C_{9,10}^{\prime\mathrm{H}^\pm}$ from Eqs. (4.4) and (4.5), we could obtain a bound on ς_d even when ς_u equals 0. Such a bound arises entirely from the information on $C_{9,10}^{\prime\mathrm{H}^\pm}$ due to the $|\varsigma_d|^2$ terms in these two Wilson coefficients (cf. Eqs. (3.18) and (3.19)). For illustration, the allowed regions in the ς_d–$M_{H^\pm}$ plane when $\varsigma_u = 0$ and in the ς_u–$M_{H^\pm}$ plane when $\varsigma_d = 0$ are shown in Fig. 4. Numerically, we obtain $|\varsigma_u| \leq 0.506$, 0.763 and 0.990, and $|\varsigma_d| \leq 212$, 476 and 622, corresponding to $M_{H^\pm} = 80$, 300 and 500 GeV, respectively. This means that the more accurate $C_{9,10}^{\prime\mathrm{NP}}$ can be better used to restrict the parameter ς_d.

4.3 P_2 and P_5' in the A2HDM

In this subsection, with the constrained parameter space for ς_u and ς_d, we investigate the impact of A2HDM on the angular observables P_2 and P_5' in the decay $B^0 \to K^{*0}\mu^+\mu^-$. As there are involved only three model parameters ς_u, ς_d and $M_{H^\pm}$ in Eqs. (3.14)–(3.19), the five Wilson coefficients ($C_7^{\prime\mathrm{H}^\pm}$ is neglected because $\bar{m}_s \ll \bar{m}_b$) are expected to be highly correlated with each other. Using the allowed values of ς_u and ς_d with three benchmark values of charged-scalar mass obtained in the previous subsection, we show in Fig. 5 the correlations among these five Wilson coefficients. One can see that, while $C_7^{\mathrm{H}^\pm}$ is hardly correlated with the other four Wilson coefficients (Fig. 5a–d), $C_9^{\mathrm{H}^\pm}$ and $C_{10}^{\mathrm{H}^\pm}$ are obviously linearly correlated with each other and the slope depends only on the charged-scalar mass $M_{H^\pm}$ (Fig. 5e), with the blue, red, and green lines obtained with $M_{H^\pm} = 80$, 300, and 500 GeV, respectively. In addition, $C_9^{\prime\mathrm{H}^\pm}$ and $C_{10}^{\prime\mathrm{H}^\pm}$ are found to be approximately linearly correlated with each other (Fig. 5f), and the slope starts to be nearly a constant when $M_{H^\pm} \geq 250$ GeV, which explains why the two lines with $M_{H^\pm} = 300$ and 500 GeV almost overlap completely in Fig. 5f. In fact, from the analytic expressions for these Wilson coefficients (cf. Eqs. (3.15)–(3.16) and (3.18)–(3.19), together with (B.3)–(B.10)), we find that $C_9^{\mathrm{H}^\pm}/C_{10}^{\mathrm{H}^\pm} \to -1 + 4\sin^2\theta_W\,[1 + 4/(9x_t)]$ and $C_9^{\prime\mathrm{H}^\pm}/C_{10}^{\prime\mathrm{H}^\pm} \to -1 + 4\sin^2\theta_W$ when $M_{H^\pm}$ goes to infinity. This explains why the lines shown in Fig. 5e, f get closer to each other with larger $M_{H^\pm}$.

The most interesting results are shown in Fig. 5g–j, which suggest that the charged scalars cannot affect the left- and right-handed semileptonic operators at the same time, under the constraints shown in Figs. 2 and 3. According to Eqs. (3.15) and (3.16), sizable $C_{9,10}^{\mathrm{H}^\pm}$ need a large $|\varsigma_u|$, which in turn implies that $|\varsigma_d|$ cannot be too large due to the constraints shown in Figs. 2 and 3. Together with the small factor $\bar{m}_b\bar{m}_s/M_W^2$ and the preset range $|\varsigma_u| \leq 2$, this renders the coefficients $C_{9,10}^{\prime\mathrm{H}^\pm}$ quite small (cf. Eqs. (3.18)–(3.19)). The same argument applies to the opposite case: sizable $C_{9,10}^{\prime\mathrm{H}^\pm}$ are possible only with a large $|\varsigma_d|$, which then implies a small $|\varsigma_u|$, resulting in quite small $C_{9,10}^{\mathrm{H}^\pm}$. These qualitative analyses explain the strong correlations observed in Fig. 5g–j, and motivate us to consider the following two specific cases for the NP Wilson coefficients:

$$\text{Case } A\text{: } C_{7,9,10}^{\mathrm{H}^\pm} \text{ are sizable, but } C_{9,10}^{\prime\mathrm{H}^\pm} \simeq 0; \tag{4.6}$$

$$\text{Case } B\text{: } C_7^{\mathrm{H}^\pm} \text{ and } C_{9,10}^{\prime\mathrm{H}^\pm} \text{ are sizable, but } C_{9,10}^{\mathrm{H}^\pm} \simeq 0. \tag{4.7}$$

They are associated to the (large $|\varsigma_u|$, small $|\varsigma_d|$) and (small $|\varsigma_u|$, large $|\varsigma_d|$) regions, respectively.

In Fig. 6, we show our predictions for the two angular observables P_2 and P_5' at large recoil both within the SM and in the A2HDM, with the Wilson coefficients obtained in the above two cases, together with the experimental data from the LHCb [11,16], Belle [17] and BaBar [118] collaborations. Here we follow closely the method used in

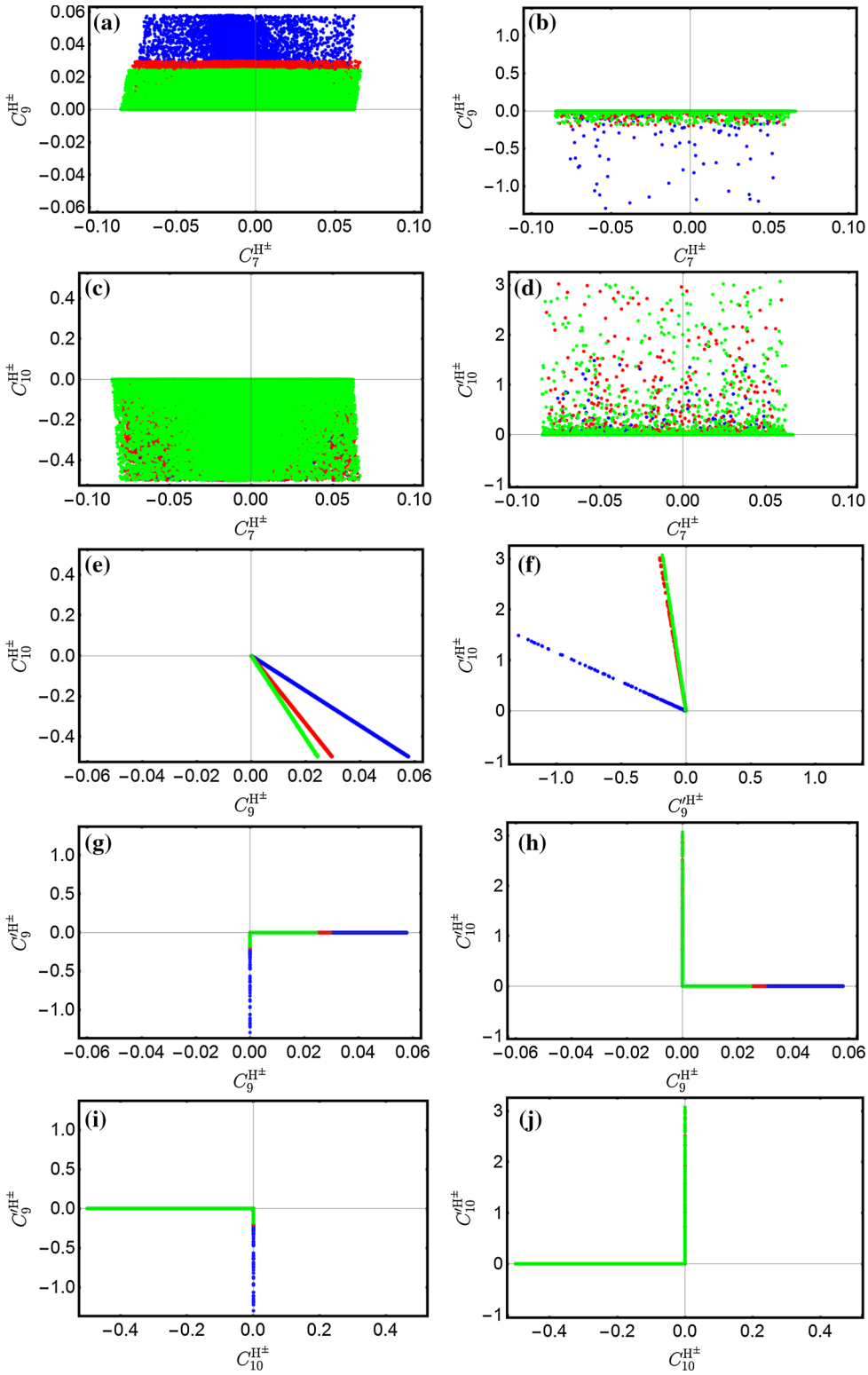

Fig. 5 Correlations among the five Wilson coefficients using the allowed values of ς_u and ς_d with three benchmark values of charged-scalar mass obtained in the previous subsection. The other captions are the same as in Fig. 2

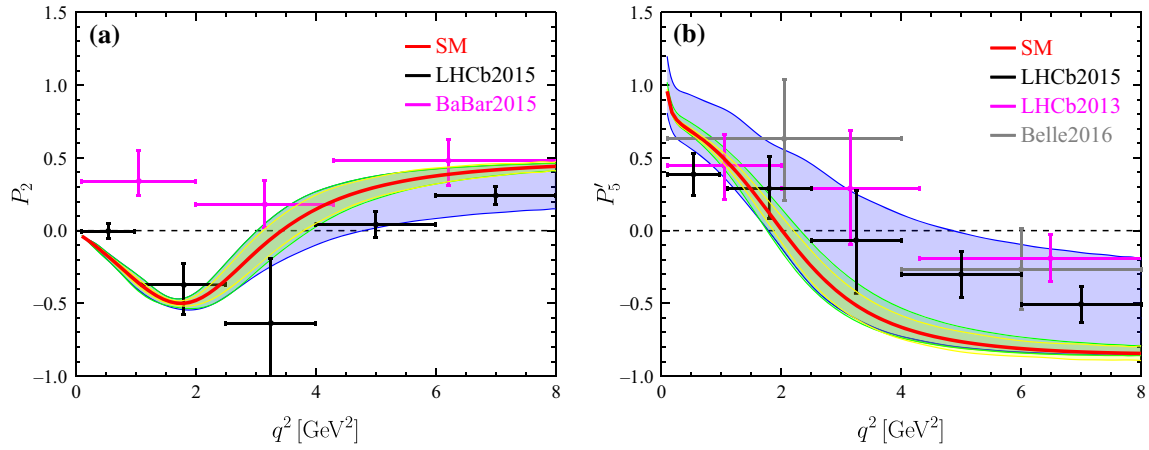

Fig. 6 The q^2 dependence of the angular observables P_2 and P_5', both within the SM (central value by a *red curve* and its uncertainty by a *yellow band*) and in the A2HDM (the *green* and *blue bands* correspond to the case A and case B, respectively). The experimental data from the LHCb [11,16], Belle [17] and BaBar [118] collaborations are represented by the corresponding *error bars* in different q^2 bins

Table 2 The zero-crossing points of P_2 (nonzero one) and P_5' both within the SM and in the A2HDM

	SM	Case A	Case B
$q_0^2(P_2)$	$3.43^{+0.33}_{-0.32}$	(3.02, 3.90)	(3.02, 4.79)
$q_0^2(P_5')$	$2.02^{+0.19}_{-0.15}$	(1.77, 2.32)	(1.79, 4.85)

Refs. [6,13,18]: Firstly, we take as input the combined LCSR-lattice fit results for the $B \to K^*$ transition form factors provided in Ref. [13], which allow us to retain all the correlated uncertainties among these form factors. Secondly, we have included the hadronic uncertainties due to non-factorizable power corrections associated with the non-perturbative charm loops [13,30], the latest discussions of which could be found in Refs. [119,120]. Finally, these two angular observables are computed within the SM, with their respective uncertainties obtained by adding in quadrature the individual uncertainty due to the $B \to K^*$ form factors, the non-factorizable charm-loop contributions, and the parametric input (mainly from $m_b(\bar{m}_b) = 4.18^{+0.04}_{-0.03}$ GeV and $m_c = 1.4 \pm 0.2$ GeV). For the NP contributions, however, we consider only the uncertainties of the model parameters and perform a random flat scan within their allowed regions. One can see clearly that there is only a small impact on P_2 and P_5' in case A, where the chirality-flipped operators $O_{9,10}'$ are absent, while in case B P_5' could be increased significantly to be consistent with the experimental data and reduce P_2 when the dimuon invariant mass squared q^2 is higher than the zero-crossing point q_0^2. Numerical results for the zero-crossing points of P_2 (nonzero one) and P_5' are given in Table 2, both within the SM and in the A2HDM. It is observed that the impact on q_0^2 in case B is more pronounced than in case A.

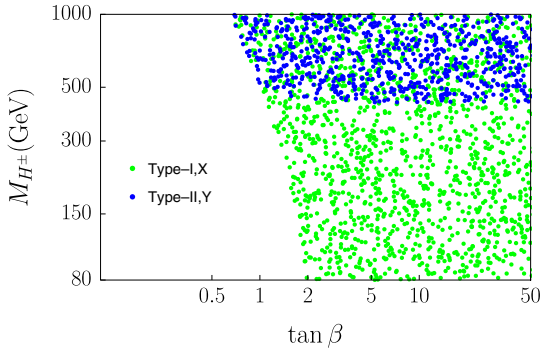

Fig. 7 Allowed regions in the $\tan\beta - M_{H^\pm}$ plane corresponding to different $\mathcal{Z}_2$-symmetric 2HDMs, under the constraint from Eq. (4.3) as well as the bounds on $C_{9,10}^{\mathrm{H}^\pm}$ and $C_{9,10}'^{\mathrm{H}^\pm}$ from Eqs. (4.4) and (4.5)

4.4 2HDMs with $\mathcal{Z}_2$ symmetries

In the generic 2HDMs with discrete $\mathcal{Z}_2$ symmetries, the three alignment parameters ς_f will be reduced to a single parameter $\tan\beta = v_2/v_1 \geq 0$, as indicated in Table 1. There are, therefore, only two model parameters, $\tan\beta$ and $M_{H^\pm}$, in the Wilson coefficients $C_{7,9,10}^{(\prime)\mathrm{H}^\pm}$. We show in Fig. 7 the allowed regions in the $\tan\beta$–$M_{H^\pm}$ plane corresponding to the four different types of 2HDMs with $\mathcal{Z}_2$ symmetries. As $C_{7,9,10}^{(\prime)\mathrm{H}^\pm}$ do not depend on the parameter ς_ℓ, the type I (II) and type X (Y) models are indistinguishable from each other. However, one can clearly distinguish types I and X from types II and Y models. As shown in Fig. 7, the bound $M_{H^\pm} > 432$ GeV is obtained for types II and Y 2HDMs, while there is no further bound found for $M_{H^\pm}$ in types I and X 2HDMs with sizable $\tan\beta$.

With the constrained model parameters shown in Fig. 7, we then show in Fig. 8 the q^2 dependence of P_2 and P_5'

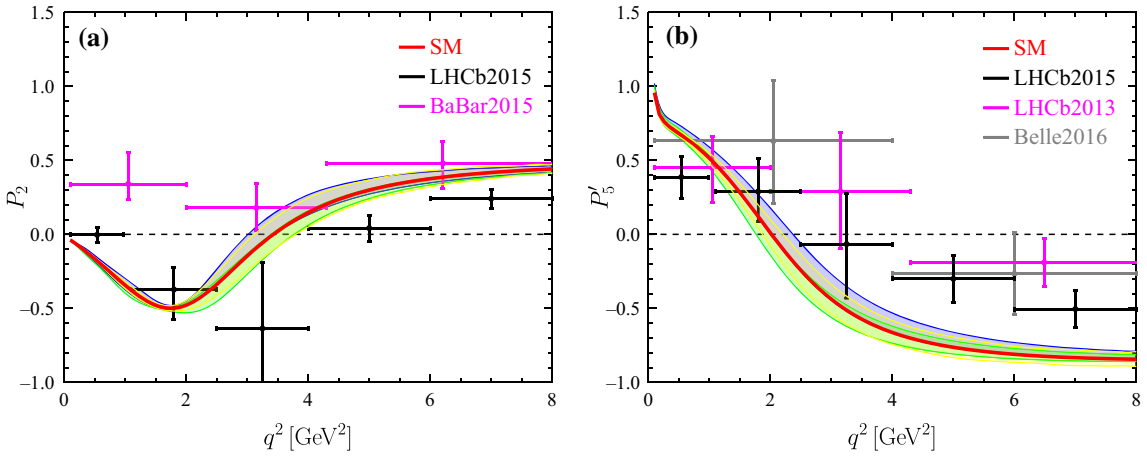

Fig. 8 The q^2 dependence of the angular observables P_2 and P_5' in the types I and X (the *green band*) and the types II and Y (the *blue band*) 2HDMs. The other captions are the same as in Fig. 6.

in the four different types of 2HDMs with $\mathcal{Z}_2$ symmetries. One can see that, compared with the SM predictions, both P_2 and P_5' are reduced in the types I and X (the green band), but increased in the types II and Y (the blue band) 2HDMs, only by a small amount. This is because the charged-scalar effect on the left- and right-handed semileptonic operators is controlled by the same parameter $\tan\beta$ and, under the constraint shown in Fig. 7, sizable $C_{9,10}^{\prime \mathrm{H}^\pm}$ are not allowed in these models. It is, therefore, concluded the 2HDMs with $\mathcal{Z}_2$ symmetries cannot explain the so-called P_5' anomaly.

5 Conclusions

In this paper, we have presented a complete one-loop calculation of the SD Wilson coefficients $C_{7,9,10}^{(\prime)\mathrm{H}^\pm}$ due to the charged-scalar exchanges through the Z^0- and γ-penguin diagrams within the A2HDM. For $C_{9,10}^{\prime \mathrm{H}^\pm}$, although being suppressed by the factor $\bar{m}_b\,\bar{m}_s/M_W^2$, they could play an important role in interpreting the observed P_5' anomaly in the decay $B^0 \to K^{*0}\mu^+\mu^-$, when the model parameter $|\varsigma_d|$ is large.

Under the constraints from the branching ratio $\mathcal{B}(B \to X_s\gamma)$ and the recent global fit results of $b \to s\ell^+\ell^-$ data, we have obtained the allowed parameter spaces in the ς_u–ς_d plane, corresponding to three representative charged-scalar masses. We found that $C_{9,10}^{\mathrm{H}^\pm}$ play a major role in the small $|\varsigma_d|$ region ($|\varsigma_d| < 1$), while $C_{9,10}^{\prime \mathrm{H}^\pm}$ are most important when the model parameter ς_u approaches 0. When ς_u is far away from 0 and $|\varsigma_d| \geq 1$, on the other hand, the impact of $C_7^{\mathrm{H}^\pm}$ will become more significant. Within the constrained parameter space, numerically, the effects of these NP Wilson coefficients can be divided into the following two cases: (A) $C_{7,9,10}^{\mathrm{H}^\pm}$ are sizable, but $C_{9,10}^{\prime \mathrm{H}^\pm} \simeq 0$, corresponding to the (large $|\varsigma_u|$, small $|\varsigma_d|$) region; (B) $C_7^{\mathrm{H}^\pm}$ and $C_{9,10}^{\prime \mathrm{H}^\pm}$ are sizable, but $C_{9,10}^{\mathrm{H}^\pm} \simeq 0$, corresponding to the (small $|\varsigma_u|$, large $|\varsigma_d|$) region. We have then discussed their impacts on the angular observables P_2 and P_5' in the decay $B^0 \to K^{*0}\mu^+\mu^-$. It is found that there is only a small impact on P_2 and P_5' in case A, while case B could obviously increase P_5' to be consistent with the experimental data and reduce P_2 when the dimuon invariant mass squared q^2 is higher than the zero-crossing point.

Finally, we have explored the constraints on $\tan\beta$ and $M_{H^\pm}$ in four types of $\mathcal{Z}_2$-symmetric 2HDMs. The role of chirality-flipped operators $O_{9,10}'$ becomes much more important for large values of $\tan\beta$. Even with the current data, the types I and X and types II and Y could be clearly distinguished from each other. However, the charged-scalar effect on P_2 and P_5' in these models is found to be small and does not help to explain the so-called P_5' anomaly.

Future precise measurements of the angular observables in $b \to s\ell^+\ell^-$ decays, especially with a finer binning of q^2, would be very helpful to provide a more definite answer concerning the observed anomalies by the LHCb and Belle collaborations, restricting further or even deciphering the NP models.

Acknowledgements The work is supported by the National Natural Science Foundation of China (NSFC) under contract Nos. 11675061, 11435003, 11225523 and 11521064. Q.H. is supported by the Excellent Doctorial Dissertation Cultivation Grant from CCNU, under contract number 2013YBZD19.

A Basic function

The basic functions $F_i(x)$ introduced in Eqs. (3.12) and (3.13) are defined, respectively, as

$$F_0(x) = \ln x, \tag{A.1}$$

$$F_1(x) = \frac{x}{4-4x} + \frac{x\ln x}{4(x-1)^2}, \tag{A.2}$$

$$F_2(x) = \frac{x}{96(x-1)} - \frac{x^2\ln x}{96(x-1)^2}, \tag{A.3}$$

$$F_3(x) = \frac{x}{8}\left[\frac{x-6}{x-1} + \frac{(3x+2)\ln x}{(x-1)^2}\right], \tag{A.4}$$

$$F_4(x) = -\frac{3x(x-3)}{32(x-1)} + \frac{x(x^2-8x+4)\ln x}{16(x-1)^2}, \tag{A.5}$$

$$F_5(x) = \frac{-19x^3+25x^2}{36(x-1)^3} + \frac{(5x^2-2x-6)x^2\ln x}{18(x-1)^4}, \tag{A.6}$$

$$F_6(x) = \frac{8x^3+5x^2-7x}{12(x-1)^3} - \frac{(3x-2)x^2\ln x}{2(x-1)^4}, \tag{A.7}$$

$$F_7(x) = \frac{x(53x^2+8x-37)}{108(x-1)^4} + \frac{x(-3x^3-9x^2+6x+2)\ln x}{18(x-1)^5}, \tag{A.8}$$

$$F_8(x) = \frac{x(18x^4+253x^3-767x^2+853x-417)}{540(x-1)^5} - \frac{x(3x^4-6x^3+3x^2+2x-3)\ln x}{9(x-1)^6}. \tag{A.9}$$

B Wilson coefficients in A2HDM

The coefficients of the different combinations of the couplings ς_u and ς_d in Eqs. (3.14)–(3.19) are given, respectively, by

$$C_{7,\,\mathrm{uu}} = -\frac{1}{6}F_6(y_t), \tag{B.1}$$

$$C_{7,\,\mathrm{ud}} = -\frac{4}{3}F_1(y_t) - \frac{80}{17}F_2(y_t) - \frac{3}{17}F_5(y_t) + \frac{1}{17}F_6(y_t), \tag{B.2}$$

$$C_{9,\,\mathrm{uu}} = \frac{8}{9}F_1(y_t) - \frac{896}{51}F_2(y_t) - \frac{1}{17}F_5(y_t) - \frac{14}{153}F_6(y_t) - \frac{x_t}{2}\left(-4+\frac{1}{\sin^2\theta_W}\right)F_1(y_t), \tag{B.3}$$

$$C_{10,\,\mathrm{uu}} = \frac{x_t}{2\sin^2\theta_W}F_1(y_t), \tag{B.4}$$

$$C'_{9,\,\mathrm{uu}} = \frac{y_t}{x_t}F_8(y_t), \tag{B.5}$$

$$C'_{9,\,\mathrm{ud}} = \frac{y_t}{x_t}F_7(y_t), \tag{B.6}$$

$$C'_{9,\,\mathrm{dd}} = \frac{y_t}{x_t}\left[\frac{2}{9}F_0(x_t) + \frac{20}{9}F_1(y_t) + \frac{928}{51}F_2(y_t) - \frac{2}{17}F_5(y_t) - \frac{11}{153}F_6(y_t)\right], \tag{B.7}$$

$$C'_{10,\,\mathrm{uu}} = -\frac{1}{17}[80F_2(y_t) + 3F_5(y_t) - F_6(y_t)], \tag{B.8}$$

$$C'_{10,\,\mathrm{ud}} = \frac{1}{\sin^2\theta_W}\left[-\frac{1}{12}F_1(y_t) + \frac{30}{17}F_2(y_t) + \frac{9}{136}F_5(y_t) - \frac{3}{136}F_6(y_t)\right] - \frac{1}{6}\left(-4+\frac{1}{\sin^2\theta_W}\right)F_1(y_t), \tag{B.9}$$

$$C'_{10,\,\mathrm{dd}} = -\frac{1}{\sin^2\theta_W}\left[\frac{1}{2}F_1(y_t) + F_2(y_t)\right] + \left(-4+\frac{1}{\sin^2\theta_W}\right)F_2(y_t), \tag{B.10}$$

and for the Wilson coefficient $C_8^{\mathrm{H}^\pm}$, we have [89]

$$C_{8,\,\mathrm{uu}} = \frac{1}{34}[720F_2(y_t) + 27F_5(y_t) + 8F_6(y_t)], \tag{B.11}$$

$$C_{8,\,\mathrm{ud}} = 2F_1(y_t) - \frac{1}{17}[240F_2(y_t) + 9F_5(y_t) - 3F_6(y_t)]. \tag{B.12}$$

References

1. S.L. Glashow, J. Iliopoulos, L. Maiani, Weak interactions with lepton–hadron symmetry. Phys. Rev. D **2**, 1285–1292 (1970)
2. T. Blake, G. Lanfranchi, D.M. Straub, Rare B decays as tests of the standard model. Prog. Part. Nucl. Phys. **92**, 50–91 (2017). arXiv:1606.00916
3. M. Beneke, T. Feldmann, D. Seidel, Systematic approach to exclusive $B \to Vl^+l^-$, $V\gamma$ decays. Nucl. Phys. B **612**, 25–58 (2001). arXiv:hep-ph/0106067
4. M. Beneke, T. Feldmann, D. Seidel, Exclusive radiative and electroweak $b \to d$ and $b \to s$ penguin decays at NLO. Eur. Phys. J. C **41**, 173 (2005). arXiv:hep-ph/0412400
5. B. Grinstein, D. Pirjol, Exclusive rare $B \to K^*\ell^+\ell^-$ decays at low recoil: controlling the long-distance effects. Phys. Rev. D **70**, 114005 (2004). arXiv:hep-ph/0404250
6. W. Altmannshofer, P. Ball, A. Bharucha, A.J. Buras, D.M. Straub, M. Wick, Symmetries and asymmetries of $B \to K^*\mu^+\mu^-$ decays in the standard model and beyond. JHEP **01**, 019 (2009). arXiv:0811.1214
7. M. Beylich, G. Buchalla, T. Feldmann, Theory of $B \to K^{(*)}\ell^+\ell^-$ decays at high q^2: OPE and quark–hadron duality. Eur. Phys. J. C **71**, 1635 (2011). arXiv:1101.5118
8. S. Descotes-Genon, J. Matias, M. Ramon, J. Virto, Implications from clean observables for the binned analysis of $B \to K^*\mu^+\mu^-$ at large recoil. JHEP **01**, 048 (2013). arXiv:1207.2753
9. S. Descotes-Genon, T. Hurth, J. Matias, J. Virto, Optimizing the basis of $B \to K^*\ell^+\ell^-$ observables in the full kinematic range. JHEP **05**, 137 (2013). arXiv:1303.5794
10. J. Gratrex, M. Hopfer, R. Zwicky, Generalised helicity formalism, higher moments and the $B \to K_{J_K}(\to K\pi)\bar{\ell}_1\ell_2$ angular distributions. Phys. Rev. D **93**(5), 054008 (2016). arXiv:1506.03970
11. LHCb Collaboration, R. Aaij et al., Measurement of form-factor-independent observables in the decay $B^0 \to K^{*0}\mu^+\mu^-$. Phys. Rev. Lett. **111**, 191801 (2013). arXiv:1308.1707

12. S. Descotes-Genon, L. Hofer, J. Matias, J. Virto, On the impact of power corrections in the prediction of $B \to K^* \mu^+ \mu^-$ observables. JHEP **12**, 125 (2014). arXiv:1407.8526
13. A. Bharucha, D.M. Straub, R. Zwicky, $B \to V \ell^+ \ell^-$ in the standard model from light-cone sum rules. JHEP **08**, 098 (2016). arXiv:1503.05534
14. S. Jäger, J. Martin Camalich, On $B \to V \ell\ell$ at small dilepton invariant mass, power corrections, and new physics. JHEP **05**, 043 (2013). arXiv:1212.2263
15. S. Jäger, J. Martin Camalich, Reassessing the discovery potential of the $B \to K^* \ell^+ \ell^-$ decays in the large-recoil region: SM challenges and BSM opportunities. Phys. Rev. D **93**(1), 014028 (2016). arXiv:1412.3183
16. LHCb Collaboration, R. Aaij et al., Angular analysis of the $B^0 \to K^{*0} \mu^+ \mu^-$ decay using 3 fb^{-1} of integrated luminosity. JHEP**02**, 104 (2016). arXiv:1512.04442
17. Belle Collaboration, A. Abdesselam et al., Angular analysis of $B^0 \to K^*(892)^0 \ell^+ \ell^-$. In: Proceedings, LHCSki 2016—a first discussion of 13 TeV results: Obergurgl, Austria, April 10–15, 2016 (2016). arXiv:1604.04042
18. W. Altmannshofer, D.M. Straub, New physics in $b \to s$ transitions after LHC run 1. Eur. Phys. J. C **75**(8), 382 (2015). arXiv:1411.3161
19. S. Descotes-Genon, L. Hofer, J. Matias, J. Virto, Global analysis of $b \to s\ell\ell$ anomalies. JHEP **06**, 092 (2016). arXiv:1510.04239
20. T. Hurth, F. Mahmoudi, S. Neshatpour, On the anomalies in the latest LHCb data. Nucl. Phys. B **909**, 737–777 (2016). arXiv:1603.00865
21. T. Hurth, F. Mahmoudi, On the LHCb anomaly in B $\to K^* \ell^+ \ell^-$. JHEP **04**, 097 (2014). arXiv:1312.5267
22. S. Descotes-Genon, J. Matias, J. Virto, Understanding the $B \to K^* \mu^+ \mu^-$ Anomaly. Phys. Rev. D **88**, 074002 (2013). arXiv:1307.5683
23. W. Altmannshofer, D.M. Straub, New physics in $B \to K^* \mu\mu$? Eur. Phys. J. C **73**, 2646 (2013). arXiv:1308.1501
24. F. Beaujean, C. Bobeth, D. van Dyk, Comprehensive Bayesian analysis of rare (semi)leptonic and radiative B decays. Eur. Phys. J. C **74**, 2897 (2014). arXiv:1310.2478. **(Erratum: Eur. Phys. J. C 74, 3179 (2014))**
25. R.R. Horgan, Z. Liu, S. Meinel, M. Wingate, Calculation of $B^0 \to K^{*0} \mu^+ \mu^-$ and $B_s^0 \to \phi \mu^+ \mu^-$ observables using form factors from lattice QCD. Phys. Rev. Lett. **112**, 212003 (2014). arXiv:1310.3887
26. T. Hurth, F. Mahmoudi, S. Neshatpour, Global fits to $b \to s\ell\ell$ data and signs for lepton non-universality. JHEP **12**, 053 (2014). arXiv:1410.4545
27. D. Du, A.X. El-Khadra, S. Gottlieb, A.S. Kronfeld, J. Laiho, E. Lunghi, R.S. Van de Water, R. Zhou, Phenomenology of semileptonic B-meson decays with form factors from lattice QCD. Phys. Rev. D **93**(3), 034005 (2016). arXiv:1510.02349
28. M. Ciuchini, M. Fedele, E. Franco, S. Mishima, A. Paul, L. Silvestrini, M. Valli, $B \to K^* \ell^+ \ell^-$ decays at large recoil in the standard model: a theoretical reappraisal. JHEP **06**, 116 (2016). arXiv:1512.07157
29. S. Meinel, D. van Dyk, Using $\Lambda_b \to \Lambda \mu^+ \mu^-$ data within a Bayesian analysis of $|\Delta B| = |\Delta S| = 1$ decays. Phys. Rev. D**94**(1), 013007 (2016). arXiv:1603.02974
30. A. Khodjamirian, T. Mannel, A.A. Pivovarov, Y.M. Wang, Charm-loop effect in $B \to K^{(*)} \ell^+ \ell^-$ and $B \to K^* \gamma$. JHEP **09**, 089 (2010). arXiv:1006.4945
31. S. Braß, G. Hiller, I. Nisandzic, Zooming in on $B \to K^* \ell\ell$ decays at low recoil. Eur. Phys. J. C **77**(1), 16 (2017). arXiv:1606.00775
32. B. Capdevila, S. Descotes-Genon, J. Matias, J. Virto, Assessing lepton-flavour non-universality from $B \to K^* \ell\ell$ angular analyses. JHEP **10**, 075 (2016). arXiv:1605.03156
33. A. Karan, R. Mandal, A. K. Nayak, R. Sinha, T.E. Browder, Signal of right-handed currents using $B \to K^* \ell^+ \ell^-$ observables at the kinematic endpoint. arXiv:1603.04355
34. I. Ahmed, M.J. Aslam, M.A. Paracha, Asymmetries in $B \to K^* \ell^+ \ell^-$ decays and two Higgs doublet model. arXiv:1602.02400
35. C.-W. Chiang, X.-G. He, G. Valencia, Z' model for $b \to s\ell\bar{\ell}$ flavor anomalies. Phys. Rev. D 93(7), 074003 (2016). arXiv:1601.07328
36. A. Celis, W.-Z. Feng, D. Lüst, Stringy explanation of $b \to s\ell^+\ell^-$ anomalies. JHEP **02**, 007 (2016). arXiv:1512.02218
37. S.M. Boucenna, A. Celis, J. Fuentes-Martin, A. Vicente, J. Virto, Non-abelian gauge extensions for B-decay anomalies. Phys. Lett. B **760**, 214–219 (2016). arXiv:1604.03088
38. A. Crivellin, J. Fuentes-Martin, A. Greljo, G. Isidori, Lepton flavor non-universality in b decays from dynamical Yukawas. Phys. Lett. B **766**, 77–85 (2017). arXiv:1611.02703
39. R. Barbieri, C.W. Murphy, F. Senia, B-decay anomalies in a composite leptoquark model. Eur. Phys. J. C **77**(1), 8 (2017). arXiv:1611.04930
40. F. Mahmoudi, T. Hurth, S. Neshatpour, Present status of $b \to s\ell^+\ell^-$ anomalies (2016). arXiv:1611.05060
41. A. Crivellin, G. D'Ambrosio, J. Heeck, Explaining $h \to \mu^\pm \tau^\mp$, $B \to K^* \mu^+ \mu^-$ and $B \to K \mu^+ \mu^- / B \to K e^+ e^-$ in a two-Higgs-doublet model with gauged $L_\mu - L_\tau$. Phys. Rev. Lett. **114**, 151801 (2015). arXiv:1501.00993
42. A. Crivellin, G. D'Ambrosio, J. Heeck, Addressing the LHC flavor anomalies with horizontal gauge symmetries. Phys. Rev. D **91**(7), 075006 (2015). arXiv:1503.03477
43. L. Calibbi, A. Crivellin, T. Ota, Effective field theory approach to $b \to s\ell\ell^{(\prime)}$, $B \to K^{(*)} \nu\bar{\nu}$ and $B \to D^{(*)} \tau\nu$ with third generation couplings. Phys. Rev. Lett. **115**, 181801 (2015). arXiv:1506.02661
44. P. Arnan, L. Hofer, F. Mescia, A. Crivellin, Loop effects of heavy new scalars and fermions in $b \to s\mu^+\mu^-$. arXiv:1608.07832
45. T.D. Lee, A theory of spontaneous T violation. Phys. Rev. D **8**, 1226–1239 (1973)
46. G.C. Branco, P.M. Ferreira, L. Lavoura, M.N. Rebelo, M. Sher, J.P. Silva, Theory and phenomenology of two-Higgs-doublet models. Phys. Rept. **516**, 1–102 (2012). arXiv:1106.0034
47. ATLAS Collaboration, G. Aad et al., Observation of a new particle in the search for the Standard Model Higgs boson with the ATLAS detector at the LHC. Phys. Lett. B **716**, 1–29 (2012). arXiv:1207.7214
48. C.M.S. Collaboration, S. Chatrchyan et al., Observation of a new boson at a mass of 125 GeV with the CMS experiment at the LHC. Phys. Lett. B **716**, 30–61 (2012). arXiv:1207.7235
49. H.E. Haber, G.L. Kane, The search for supersymmetry: probing physics beyond the standard model. Phys. Rept. **117**, 75–263 (1985)
50. J.E. Kim, Light pseudoscalars. Particle physics and cosmology. Phys. Rept. **150**, 1–177 (1987)
51. M. Trodden, Electroweak baryogenesis: a brief review. In: Proceedings, 33rd rencontres de Moriond 98 electrowek interactions and unified theories: Les racs, France, Mar 14–21, 1998, pp. 471–480 (1998). arXiv:hep-ph/9805252
52. J.F. Gunion, H.E. Haber, G.L. Kane, S. Dawson, The Higgs hunter's guide. Front. Phys. **80**, 1–404 (2000)
53. S.L. Glashow, S. Weinberg, Natural conservation laws for neutral currents. Phys. Rev. D **15**, 1958 (1977)
54. A. Pich, P. Tuzón, Yukawa alignment in the two-higgs-doublet model. Phys. Rev. D **80**, 091702 (2009). arXiv:0908.1554
55. N. Cabibbo, Unitary symmetry and leptonic decays. Phys. Rev. Lett. **10**, 531–533 (1963)
56. M. Kobayashi, T. Maskawa, CP violation in the renormalizable theory of weak interaction. Prog. Theor. Phys. **49**, 652–657 (1973)

57. W. Altmannshofer, S. Gori, G.D. Kribs, A minimal flavor violating 2HDM at the LHC. Phys. Rev. D **86**, 115009 (2012). arXiv:1210.2465
58. Y. Bai, V. Barger, L.L. Everett, G. Shaughnessy, General two Higgs doublet model (2HDM-G) and large hadron collider data. Phys. Rev. D **87**, 115013 (2013). arXiv:1210.4922
59. V. Barger, L.L. Everett, H.E. Logan, G. Shaughnessy, Scrutinizing the 125 GeV Higgs boson in two Higgs doublet models at the LHC, ILC, and muon collider. Phys. Rev. D**88**(11), 115003 (2013). arXiv:1308.0052
60. D. López-Val, T. Plehn, M. Rauch, Measuring extended Higgs sectors as a consistent free couplings model. JHEP **10**, 134 (2013). arXiv:1308.1979
61. L. Wang, X.-F. Han, Status of the aligned two-Higgs-doublet model confronted with the Higgs data. JHEP **04**, 128 (2014). arXiv:1312.4759
62. A. Celis, V. Ilisie, A. Pich, LHC constraints on two-Higgs doublet models. JHEP **07**, 053 (2013). arXiv:1302.4022
63. A. Celis, V. Ilisie, A. Pich, Towards a general analysis of LHC data within two-Higgs-doublet models. JHEP **12**, 095 (2013). arXiv:1310.7941
64. M. Jung, A. Pich, P. Tuzón, Charged-Higgs phenomenology in the aligned two-Higgs-doublet model. JHEP **11**, 003 (2010). arXiv:1006.0470
65. M. Jung, A. Pich, P. Tuzón, The $\bar{B} \to X_s\gamma$ rate and CP asymmetry within the aligned two-higgs-doublet model. Phys. Rev. D **83**, 074011 (2011). arXiv:1011.5154
66. M. Jung, X.-Q. Li, A. Pich, Exclusive radiative B-meson decays within the aligned two-Higgs-doublet model. JHEP **10**, 063 (2012). arXiv:1208.1251
67. A. Celis, M. Jung, X.-Q. Li, A. Pich, Sensitivity to charged scalars in $B \to D^{(*)}\tau\nu_\tau$ and $B \to \tau\nu_\tau$ decays. JHEP **01**, 054 (2013). arXiv:1210.8443
68. L. Duarte, G.A. González-Sprinberg, J. Vidal, Top quark anomalous tensor couplings in the two-Higgs-doublet models. JHEP **11**, 114 (2013). arXiv:1308.3652
69. M. Jung, A. Pich, Electric dipole moments in two-Higgs-doublet models. JHEP **04**, 076 (2014). arXiv:1308.6283
70. X.-Q. Li, J. Lu, A. Pich, $B^0_{s,d} \to \ell^+\ell^-$ decays in the aligned two-Higgs-doublet model. JHEP **06**, 022 (2014). arXiv:1404.5865
71. V. Ilisie, New Barr–Zee contributions to $(g-2)_\mu$ in two-Higgs-doublet models. JHEP **04**, 077 (2015). arXiv:1502.04199
72. G. Abbas, A. Celis, X.-Q. Li, J. Lu, A. Pich, Flavour-changing top decays in the aligned two-Higgs-doublet model. JHEP **06**, 005 (2015). arXiv:1503.06423
73. T. Han, S.K. Kang, J. Sayre, Muon $g-2$ in the aligned two Higgs doublet model. JHEP **02**, 097 (2016). arXiv:1511.05162
74. L. Wang, S. Yang, X.F. Han, $h \to \mu\tau$ and muon g-2 in the alignment limit of two-Higgs-doublet model. arXiv:1606.04408
75. S. Davidson, H.E. Haber, Basis-independent methods for the two-Higgs-doublet model. Phys. Rev. D **72**, 035004 (2005). arXiv:hep-ph/0504050. **(Erratum: Phys. Rev.D 72, 099902 (2005))**
76. H.E. Haber, D. O'Neil, Basis-independent methods for the two-Higgs-doublet model. II. The significance of tanβ. Phys. Rev. D **74**, 015018 (2006). arXiv:hep-ph/0602242. **(Erratum: Phys. Rev. D 74(5), 059905 (2006))**
77. H.E. Haber, D. O'Neil, Basis-independent methods for the two-Higgs-doublet model III: the CP-conserving limit, custodial symmetry, and the oblique parameters S, T, U. Phys. Rev. D **83**, 055017 (2011). arXiv:1011.6188
78. G. Buchalla, A.J. Buras, M.E. Lautenbacher, Weak decays beyond leading logarithms. Rev. Mod. Phys. **68**, 1125–1144 (1996). arXiv:hep-ph/9512380
79. T. Inami, C.S. Lim, Effects of superheavy quarks and leptons in low-energy weak processes $K_L \to \mu\bar{\mu}$, $K^+ \to \pi^+\nu\bar{\nu}$ and $K^0 \leftrightarrow \bar{K}^0$. Prog. Theor. Phys. **65**, 297 (1981). **(Erratum: Prog. Theor. Phys. 65, 1772 (1981))**
80. M. Misiak, The $b \to se^+e^-$ and $b \to s\gamma$ decays with next-to-leading logarithmic QCD corrections. Nucl. Phys. B **393**, 23–45 (1993). **(Erratum: Nucl. Phys. B 439, 461 (1995))**
81. N.G. Deshpande, G. Eilam, Flavor-changing electromagnetic transitions. Phys. Rev. D **26**, 2463 (1982)
82. N.G. Deshpande, M. Nazerimonfared, Flavor changing electromagnetic vertex in a nonlinear R_ξ gauge. Nucl. Phys. B **213**, 390–408 (1983)
83. S.-P. Chia, An exact calculation of $\bar{d}sg$ vertex. Phys. Lett. B **130**, 315–320 (1983)
84. S.-P. Chia, G. Rajagopal, An exact calculation of the flavor changing quark–photon vertex. Phys. Lett. B **156**, 405–410 (1985)
85. S.-P. Chia, Radiative decay of the bottom quark and the $WW\gamma$ coupling. Phys. Lett. B **240**, 465–470 (1990)
86. L.-S. Wu, Z.-J. Xiao, Exact calculations of vertex $\bar{s}\gamma b$ and $\bar{s}Zb$ in the unitary gauge. Commun. Theor. Phys. **48**, 502–508 (2007). arXiv:hep-ph/0612326
87. X.-G. He, J. Tandean, G. Valencia, Penguin and box diagrams in unitary gauge. Eur. Phys. J. C **64**, 681–687 (2009). arXiv:0909.3638
88. A.J. Buras, Climbing NLO and NNLO summits of weak decays. arXiv:1102.5650
89. B. Grinstein, R.P. Springer, M.B. Wise, Strong interaction effects in weak radiative $\bar{B}$ meson decay. Nucl. Phys. B **339**, 269–309 (1990)
90. S. Bertolini, F. Borzumati, A. Masiero, G. Ridolfi, Effects of supergravity induced electroweak breaking on rare B decays and mixings. Nucl. Phys. B **353**, 591–649 (1991)
91. P.L. Cho, M. Misiak, D. Wyler, $K_L \to \pi^0 e^+e^-$ and $B \to X_s l^+l^-$ decay in the MSSM. Phys. Rev. D **54**, 3329–3344 (1996). arXiv:hep-ph/9601360
92. P.H. Chankowski, L. Slawianowska, $B^0_{d,s} \to \mu^-\mu^+$ decay in the MSSM. Phys. Rev. D **63**, 054012 (2001). arXiv:hep-ph/0008046
93. M. Ciuchini, G. Degrassi, P. Gambino, G.F. Giudice, Next-to-leading QCD corrections to $B \to X_s\gamma$: standard model and two Higgs doublet model. Nucl. Phys. B **527**, 21–43 (1998). arXiv:hep-ph/9710335
94. F. Borzumati, C. Greub, Two Higgs doublet model predictions for $\bar{B} \to X_s\gamma$ in NLO QCD. Phys. Rev. D **58**, 074004 (1998). arXiv:hep-ph/9802391. **(Addendum: Phys. Rev. D 59, 057501 (1999))**
95. C. Bobeth, M. Misiak, J. Urban, Matching conditions for $b \to s\gamma$ and $b \to sgluon$ in extensions of the standard model. Nucl. Phys. B **567**, 153–185 (2000). arXiv:hep-ph/9904413
96. C. Bobeth, A.J. Buras, F. Krüger, J. Urban, QCD corrections to $\bar{B} \to X_{d,s}\nu\bar{\nu}$, $\bar{B}_{d,s} \to \ell^+\ell^-$, $K \to \pi\nu\bar{\nu}$ and $K_L \to \mu^+\mu^-$ in the MSSM. Nucl. Phys. B **630**, 87–131 (2002). arXiv:hep-ph/0112305
97. S. Schilling, C. Greub, N. Salzmann, B. Töedtli, QCD corrections to the Wilson coefficients C_9 and C_{10} in two-Higgs doublet models. Phys. Lett. B **616**, 93–100 (2005). arXiv:hep-ph/0407323
98. F. Krüger, L.M. Sehgal, N. Sinha, R. Sinha, Angular distribution and CP asymmetries in the decays $\bar{B} \to K^-\pi^+e^-e^+$ and $\bar{B} \to \pi^-\pi^+e^-e^+$. Phys. Rev. D **61**, 114028 (2000). arXiv:hep-ph/9907386. **(Erratum: Phys. Rev. D 63, 019901 (2001))**
99. D. Bečirević, E. Schneider, On transverse asymmetries in $B \to K^*\ell^+\ell^-$. Nucl. Phys. B **854**, 321–339 (2012). arXiv:1106.3283
100. J. Matias, F. Mescia, M. Ramon, J. Virto, Complete anatomy of $\bar{B}_d \to \bar{K}^{*0}(\to K\pi)\ell^+\ell^-$ and its angular distribution. JHEP **04**, 104 (2012). arXiv:1202.4266
101. OPAL, DELPHI, L3, ALEPH, LEP Higgs Working Group for Higgs boson searches Collaboration, Search for charged Higgs bosons: preliminary combined results using LEP data collected at

energies up to 209-GeV. In: Lepton and photon interactions at high energies. Proceedings, 20th international symposium, LP 2001, Rome, Italy, July 23–28, 2001 (2001). arXiv:hep-ex/0107031
102. A. Barroso, P.M. Ferreira, I.P. Ivanov, R. Santos, Metastability bounds on the two Higgs doublet model. JHEP **06**, 045 (2013). arXiv:1303.5098
103. P.S. Bhupal Dev, A. Pilaftsis, Maximally symmetric two higgs doublet model with natural standard model alignment. JHEP**12**, 024 (2014). arXiv:1408.3405. (Erratum: JHEP 1511, 147 (2015))
104. D. Das, New limits on tan β for 2HDMs with Z_2 symmetry. Int. J. Mod. Phys. A **30**(26), 1550158 (2015). arXiv:1501.02610
105. I. Chakraborty, A. Kundu, Scalar potential of two-Higgs doublet models. Phys. Rev. D **92**(9), 095023 (2015). arXiv:1508.00702
106. C. Patrignani, Review of particle physics. *Chin. Phys. C* **40**(10), 100001 (2016)
107. CLEO Collaboration, S. Chen et al., Branching fraction and photon energy spectrum for $b \to s\gamma$. Phys. Rev. Lett. **87**, 251807 (2001). arXiv:hep-ex/0108032
108. Belle Collaboration, A. Limosani et al., Measurement of inclusive radiative B-meson decays with a photon energy threshold of 1.7-GeV. Phys. Rev. Lett. **103**, 241801 (2009). arXiv:0907.1384
109. Belle Collaboration, T. Saito et al., Measurement of the $\bar{B} \to X_s\gamma$ branching fraction with a sum of exclusive decays. Phys. Rev. D **91**(5), 052004 (2015). arXiv:1411.7198
110. BaBar Collaboration, B. Aubert et al., Measurement of the $B \to X_s\gamma$ branching fraction and photon energy spectrum using the recoil method. Phys. Rev. D **77**, 051103 (2008). arXiv:0711.4889
111. BaBar Collaboration, J.P. Lees et al., Precision measurement of the $B \to X_s\gamma$ photon energy spectrum, branching fraction, and direct CP asymmetry $A_{CP}(B \to X_{s+d}\gamma)$. Phys. Rev. Lett. **109**, 191801 (2012). arXiv:1207.2690
112. BaBar Collaboration, J.P. Lees et al., Measurement of B($B \to X_s\gamma$), the $B \to X_s\gamma$ photon energy spectrum, and the direct CP asymmetry in $B \to X_{s+d}\gamma$ decays. Phys. Rev. D **86**, 112008 (2012). arXiv:1207.5772
113. BaBar Collaboration, J.P. Lees et al., Exclusive measurements of $b \to s\gamma$ transition rate and photon energy spectrum. Phys. Rev. D **86**, 052012 (2012). arXiv:1207.2520
114. Heavy Flavor Averaging Group (HFAG) Collaboration, Y. Amhis et al., Averages of b-hadron, c-hadron, and τ-lepton properties as of summer 2014. arXiv:1412.7515
115. M. Misiak et al., Updated NNLO QCD predictions for the weak radiative B-meson decays. Phys. Rev. Lett. **114**(22), 221801 (2015). arXiv:1503.01789
116. X.Q. Li, Y.D. Yang, X.B. Yuan, Exclusive radiative B-meson decays within minimal flavor-violating two-Higgs-doublet models. Phys. Rev. D **89**, 054024 (2014). arXiv:1311.2786
117. P. Gambino, M. Gorbahn, U. Haisch, Anomalous dimension matrix for radiative and rare semileptonic B decays up to three loops. Nucl. Phys. B **673**, 238–262 (2003). hep-ph/0306079
118. BaBar Collaboration, J.P. Lees et al., Measurement of angular asymmetries in the decays $B \to K^*\ell^+\ell^-$. Phys. Rev. D **93**(5), 052015 (2016). arXiv:1508.07960
119. B. Capdevila, S. Descotes-Genon, L. Hofer, J. Matias, Hadronic uncertainties in $B \to K^*\mu^+\mu^-$: a state-of-the-art analysis. arXiv:1701.08672
120. V.G. Chobanova, T. Hurth, F. Mahmoudi, D. Martinez Santos, S. Neshatpour, Large hadronic power corrections or new physics in the rare decay $B \to K^*\mu^+\mu^-$? arXiv:1702.02234